Mon. Not. R. Astron. Soc. **382,** 177–193 (2007) doi:10.1111/j.1365-2966.2007.12235.x

A homogeneous sample of sub-damped Lyman α systems – IV. Global metallicity evolution

Céline Péroux,[1⋆] Miroslava Dessauges-Zavadsky,[2] Sandro D'Odorico,[1] Tae-Sun Kim[3] and Richard G. McMahon[4]

[1]*European Southern Observatory, Karl-Schwarzchild-Strasse 2, 85748 Garching-bei-München, Germany*
[2]*Observatoire de Genève, 1290 Sauverny, Switzerland*
[3]*Astrophysikalisches Institut Potsdam, An der Sternwarte 16, 14482 Potsdam, Germany*
[4]*Institute of Astronomy, Madingley Road, Cambridge CB3 0HA*

Accepted 2007 July 15. Received 2007 July 13; in original form 2006 November 3

ABSTRACT

An accurate method to measure the abundance of high-redshift galaxies involves the observation of absorbers along the line of sight towards a background quasar. Here, we present abundance measurements of 13 $z \geqslant 3$ sub-damped Lyman α (sub-DLA) systems (quasar absorbers with H I column density in the range $19 < \log N(\mathrm{H\,I}) < 20.3\,\mathrm{cm}^{-2}$) based on high-resolution observations with the VLT UVES spectrograph. These observations more than double the amount of metallicity information for sub-DLAs available at $z > 3$. These new data, combined with other sub-DLA measurements from the literature, confirm the stronger evolution of metallicity with redshift for sub-DLAs than for the classical damped Lyman α absorbers. In addition, these observations are used to compute for the first time, using photoionization modelling in a sample of sub-DLAs, the fraction of gas that is ionized. Based on these results, we calculate that sub-DLAs contribute no more than 6 per cent of the expected amount of metals at $z \sim 2.5$. We therefore conclude that, even if sub-DLAs are found to be more metal-rich than classical DLAs, their contribution is insufficient to solve the so-called 'missing-metals' problem.

Key words: galaxies: abundances – galaxies: high-redshift – quasars: absorption lines.

1 INTRODUCTION

Damped Lyman α systems (hereafter DLAs) seen in absorption in the spectra of background quasars are selected at any redshift, independent of their intrinsic luminosity. They have hydrogen column densities of $\log N(\mathrm{H\,I}) \geqslant 20.3$. DLAs are also contributors to the neutral gas, $\Omega(\mathrm{H\,I})$, in the Universe at high redshifts, and it is from this gas reservoir that the stars visible today formed (Wolfe et al. 1995). Furthermore, DLAs offer a direct and accurate probe of elemental abundances over >90 per cent of the age of the Universe.

Recently, much attention has been given to sub-damped Lyman α systems, a term first coined by Péroux et al. (2003a). These systems have H I column density in the range $19 < \log N(\mathrm{H\,I}) < 20.3\,\mathrm{cm}^{-2}$. In a series of papers, our group has analysed a unique homogeneous sample of sub-DLAs, all observed at the same resolution with the same instrument on the Very Large Telescope (VLT). The first two papers are based on the ESO/UVES archives (Dessauges-Zavadsky et al. 2003, hereafter Paper I; Péroux et al. 2003b, hereafter Paper II), whereas the more recent studies are from our own observational programmes (Péroux et al. 2005, hereafter Paper III; this paper, hereafter Paper IV), leading to a new sample of high-redshift sub-DLAs observed under the same conditions. These works, as well as other recent studies, suggest that high metallicities can be found more easily in sub-DLAs than in classic DLAs, especially at low redshifts (e.g. Pettini et al. 2000; Jenkins et al. 2005; Péroux et al. 2006a; Prochaska et al. 2006; Péroux et al. 2006b). In the this paper, we study a new sample of high-redshift sub-DLAs in order better to constrain their metallicities at $z > 3$. In addition, our data are used in combination with data from the literature to compute the fraction of ionized gas in a sample of sub-DLAs and to obtain a reliable estimate of the contribution of sub-DLAs to the global metallicity.

The paper is structured as follows. In Section 2, we present the methodology and results of the determination of the chemical content of these high-redshift sub-DLAs. In Section 3, the total abundances, including results from detailed photoionization models, are given, and the redshift evolution of the metallicity is presented. Finally, Section 4 describes the contribution of sub-DLAs to the global metallicity in the context of the so-called missing metals problem.

2 A SAMPLE OF 13 $z \geqslant 3$ SUB-DLAS

Table 1 summarizes the absorption redshift and $N(\mathrm{H\,I})$ column densities for each of the 13 $z \geqslant 3$ sub-DLAs in the sample under study. The data acquisition and reduction are described in Péroux et al.

⋆E-mail: cperoux@eso.org

Table 1. The sample of the 13 high-redshift sub-DLAs for which abundance studies have been undertaken.

Quasar	z_{em}	z_{abs}	$\log N(\mathrm{H\,I})$
PSS J0118+0320	4.230	4.128	20.02 ± 0.15
PSS J0121+0347	4.127	2.976	19.53 ± 0.10
SDSS J0124+0044	3.840	2.988	19.18 ± 0.10
...	...	3.078	20.21 ± 0.10
PSS J0133+0400	4.154	3.139	19.01 ± 0.10
...	...	3.995	19.94 ± 0.15
...	...	3.999	19.16 ± 0.15
...	...	4.021	19.09 ± 0.15
BRI J0137−4224	3.970	3.101	19.81 ± 0.10
...	...	3.665	19.11 ± 0.10
BR J2215−1611	3.990	3.656	19.01 ± 0.15
...	...	3.662	20.05 ± 0.15
BR J2216−6714	4.469	3.368	19.80 ± 0.10

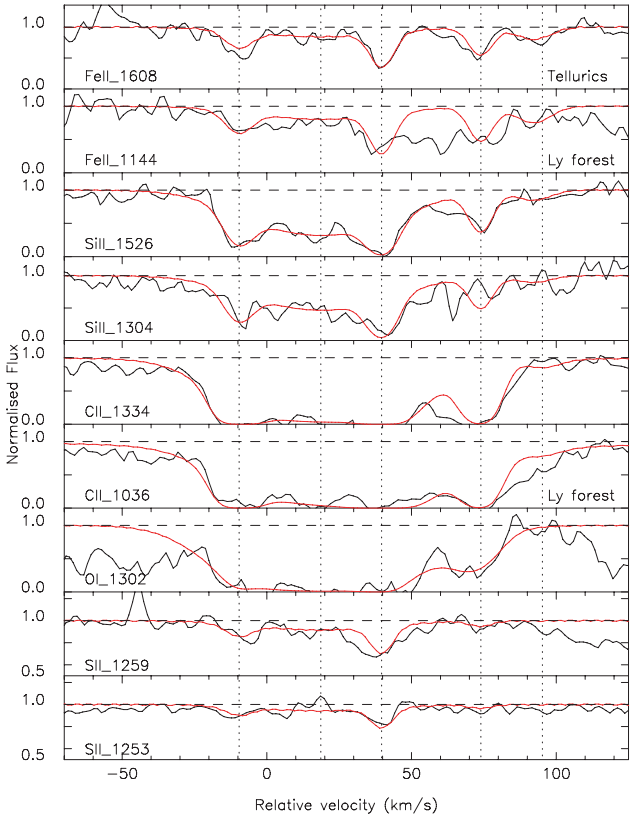

Figure 1. Fit to the low-ionization transitions of the $z_{abs} = 4.128$, $\log N(\mathrm{H\,I}) = 20.02 \pm 0.15$ sub-DLA towards PSS J0118+0320 (see Table 2). In this and the following figures, the zero velocity corresponds to the absorption redshift listed in Table 1, the vertical dashed lines correspond to the fitted components, 'Ly forest' indicates that the metal line falls in the Lyman α forest of the quasar spectrum, and 'Tellurics' indicates a region contaminated by telluric lines.

(2005). In the case of PSS J0133+0400, our own data have been supplemented by a 3000-s exposure with setting 860 (ESO 74.A-0306, P.I.: Valentina D'Odorico) and a 5200-s exposure with setting 540 (ESO 73.A-0071, P.I.: Cédric Ledoux).

In this section, details of each of the studied sub-DLAs are provided. We searched for metals associated with the Lyman lines over the spectral coverage available, and looked for more than the 40 transitions most frequently detected in high-column-density quasar absorbers. The metal column densities were then determined by fitting Voigt profiles to the absorption lines. The fits were performed using the χ^2 minimization routine FITLYMAN in MIDAS (Fontana & Ballester 1995).

(i) **PSS J0118+0320** ($z_{em} = 4.230$, $z_{abs} = 4.128$, $\log N(\mathrm{H\,I}) = 20.02 \pm 0.15$)

With $\log N(\mathrm{H\,I}) = 20.02 \pm 0.15$, this system is at the high end of the sub-DLA definition. Many metal lines are detected at $z_{abs} = 4.128$, some of which are clearly saturated. The fit was performed using Fe II $\lambda\lambda$1608, 1144, and Si II $\lambda\lambda$1526, 1304, 1259 and 1253 simultaneously to derive the redshifts and b parameters of the five components. The fit is shown in Fig. 1, and the matching parameters are presented in Table 2. In this and the following tables, velocities and b are in km s^{-1}, and the values for N are in cm^{-2}. Lower limits for C II and O I are derived from the saturated lines. The Zn II λ2026 line is covered by our spectrum but is situated in a region too noisy to allow the derivation of any meaningful upper limit.

Both Si IV and C IV high-ionization doublets are detected. The redshifts and b of the nine components are derived from a simultaneous fit of C IV $\lambda\lambda$1548, 1550 and Si IV λ1393 (Si IV λ1402 is affected by telluric lines). The resulting fit is overplotted on Si IV λ1402 for a consistency check. The fit is shown in Fig. 2, and the matching parameters are presented in Table 3.

(ii) **PSS J0121+0347** ($z_{em} = 4.127$, $z_{abs} = 2.976$, $\log N(\mathrm{H\,I}) = 19.53 \pm 0.10$)

The low-ionization transitions in this system are well fitted with one component, the redshift and b of which are fixed by a simultaneous fit of Si II λ1260, O I λ1302, C II λ1334, Fe II λ 1608 and Al II λ1670. The first four lines are situated in the Lyman α forest. This explains the likely blending that affects them. Measurements from Si III, O I and C II are therefore considered as upper limits. The fit is shown in Fig. 3, and the matching parameters are presented in Table 4. Al III $\lambda\lambda$1854 and 1862 are covered but not detected. An upper limit is derived for the Al abundance: $\log N(\mathrm{Al\,III}) < 11.77$ at 4σ.

Interestingly, in this system the high-ionization transitions are partially fitted with the same velocity component as used for the low-ionization transitions. The C IV and Si IV doublets are fitted simultaneously. C IV is heavily blended and therefore leads to an upper limit, whereas Si IV is nicely fitted from the Si IV λ1393 line. The fit is shown in Fig. 4, and the matching parameters are presented in Table 5.

(iii) **SDSS J0124+0044** ($z_{em} = 3.840$, $z_{abs} = 2.988$, $\log N(\mathrm{H\,I}) = 19.18 \pm 0.10$)

This system has low-ionization lines that cover a large velocity range, and the profiles are well characterized by two distinct clumps at ~ -100 and $\sim +30$ km s^{-1}. A simultaneous fit to Al II λ1670 and Si II λ1526 is used to derive the redshifts and values of b of the four components in the low-ionization transitions of the sub-DLA at $z_{abs} = 2.988$ towards SDSS J0124+0400. These results are checked for consistency with various other Si II lines (Si II $\lambda\lambda$1193, 1190, 1260 and Si II $\lambda\lambda$1526, 1808 are not covered by our data). The same redshifts and values of b are used to derive the column density of C II λ1334 and upper limits from S II $\lambda\lambda$1253, 1259 and Fe III λ1122, which are all probably blended by lines from the Lyman α forest. Similarly, an upper limit is derived for Fe II using the many lines falling in the forest (Fe II $\lambda\lambda$1063, 1096, 1121, 1125, 1143 and 1144) as well as Fe II λ1608. The fit is shown in Fig. 5, and the

Table 2. Parameters fitted to the low-ionization transitions of the $z_{abs} = 4.128$, log N(H I) $= 20.02 \pm 0.15$ sub-DLA towards PSS J0118+0320.

z	b	log N(Fe II)	log N(Si II)	log N(C II)	log N(O I)	log N(S II)
4.127836	4.61 ± 0.14	13.21 ± 0.11	13.60 ± 0.02	>15.35	>13.95	13.41 ± 0.11
4.128319	30.06 ± 0.21	13.57 ± 0.12	14.14 ± 0.02	>14.58	>15.15	13.94 ± 0.11
4.128678	3.11 ± 0.14	13.71 ± 0.11	14.69 ± 0.04	>17.28	>16.37	13.75 ± 0.11
4.129264	3.30 ± 0.18	13.43 ± 0.12	13.42 ± 0.02	>15.64	>14.02	13.02 ± 0.13
4.129627	6.87 ± 0.25	13.12 ± 0.11	12.73 ± 0.01	>12.60	>12.00	11.89 ± 0.12

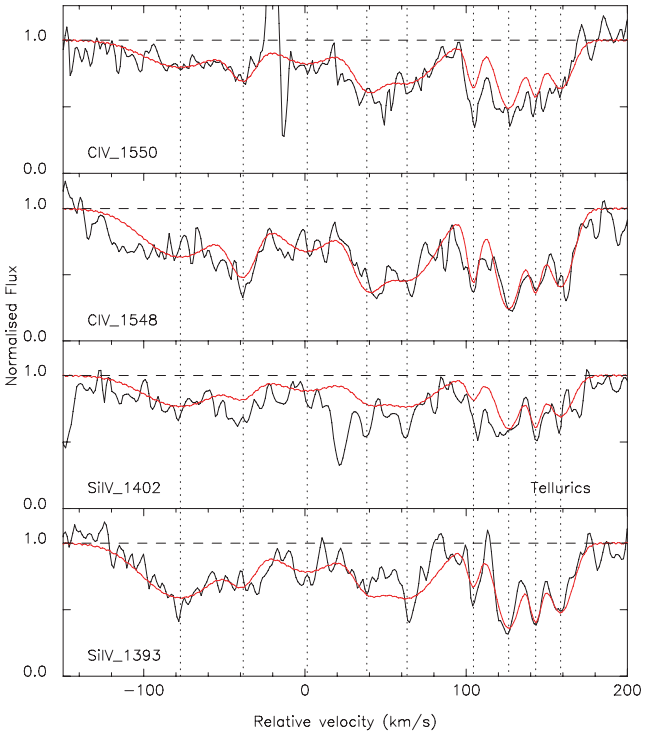

Figure 2. Fit to the high-ionization transitions of the $z_{abs} = 4.128$, log N(H I) $= 20.02 \pm 0.15$ sub-DLA towards PSS J0118+0320 (see Table 3).

matching parameters are presented in Table 6. The two Al III lines are not covered by our spectrum for this system.

The C IV doublet is nicely fitted with seven components, the two first being the strongest. The Si IV doublet is blended but is nevertheless fitted using the same components in order to derive an upper limit on the abundance. Note, however, that there is no physical reason to suggest that C IV and Si IV should come from the same region, i.e. that they should have the same velocity profile. It is just an empirical fact that in DLAs this is often the case. The fit is shown in Fig. 6, and the matching parameters are presented in Table 7.

(iv) **SDSS J0124+0044** ($z_{em} = 3.840$, $z_{abs} = 3.078$, log N(H I) $= 20.21 \pm 0.10$)

This system has a fairly high H I column density of log N(H I) $= 20.21 \pm 0.10$. The Si II $\lambda\lambda$1304 and 1526 profiles of the sub-DLA at $z_{abs} = 3.078$ are well fitted by two components. The results of this simultaneous fit are applied to the blended Si II $\lambda\lambda$1190, 1193 and 1260 for a consistency check. The same redshifts and values of b are used to derive limits on O I λ1302, C II λ1334 and Fe II $\lambda\lambda$1096, 1125, 1144 and 1608. O I and C II are clearly saturated and lead to lower limits. The column density for Fe II λ is constrained from a combination of the red wing of Fe II λ1608 and the blue wing of Fe II

Table 3. Parameters fitted to the high-ionization transitions of the $z_{abs} = 4.128$, log N(H I) $= 20.02 \pm 0.15$ sub-DLA towards PSS J0118+0320.

z	b	log N(C IV)	log N(Si IV)
4.126680	29.70 ± 0.26	13.49 ± 0.12	13.17 ± 0.12
4.127345	9.90 ± 0.13	13.19 ± 0.12	12.47 ± 0.12
4.128024	22.20 ± 0.31	13.30 ± 0.11	12.71 ± 0.22
4.128656	11.10 ± 0.12	13.30 ± 0.33	12.56 ± 0.12
4.129083	21.60 ± 0.23	13.59 ± 0.11	13.04 ± 0.11
4.129787	3.20 ± 0.02	13.04 ± 0.12	12.30 ± 0.12
4.130161	8.70 ± 0.04	13.50 ± 0.11	12.97 ± 0.12
4.130446	2.60 ± 0.01	13.08 ± 0.12	12.65 ± 0.12
4.130711	9.00 ± 0.08	13.31 ± 0.11	12.84 ± 0.12

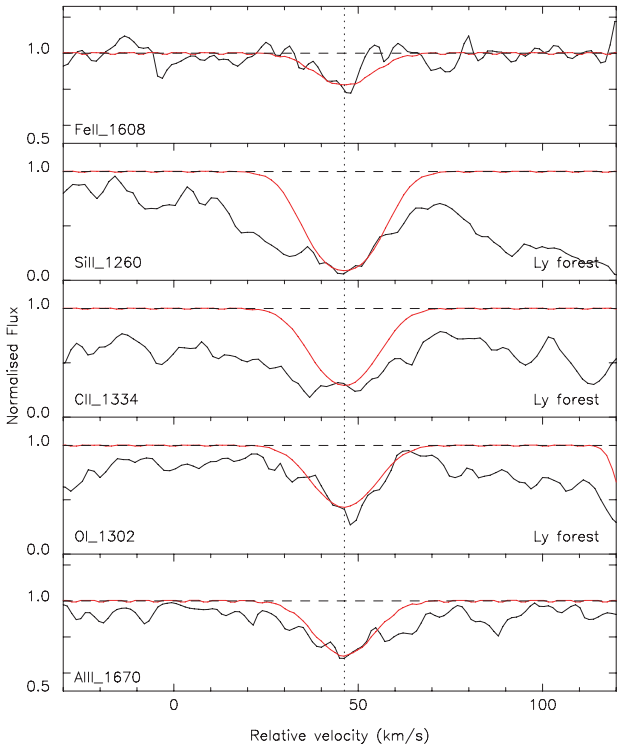

Figure 3. Fit to the low-ionization transitions of the $z_{abs} = 2.976$, log N(H I) $= 19.53 \pm 0.10$ sub-DLA towards PSS J0121+0347 (see Table 4).

λ1096 and is consistent with all the other Fe II λ lines available. The fit is shown in Fig. 7, and the matching parameters are presented in Table 8.

The Si IV doublet associated with this system is totally blended in the forest, but the C IV seems to be detected as an extremely broad

Table 4. Parameters fitted to the low-ionization transitions of the $z_{abs} = 2.976$, $\log N(\mathrm{H\,I}) = 19.53 \pm 0.10$ sub-DLA towards PSS J0121+0347.

z	b	$\log N$(Fe II)	$\log N$(Si II)	$\log N$(C II)	$\log N$(O I)	$\log N$(Al III)
2.976613	9.90 ± 0.94	13.18 ± 0.30	<13.15	<13.72	<13.98	11.93 ± 0.32

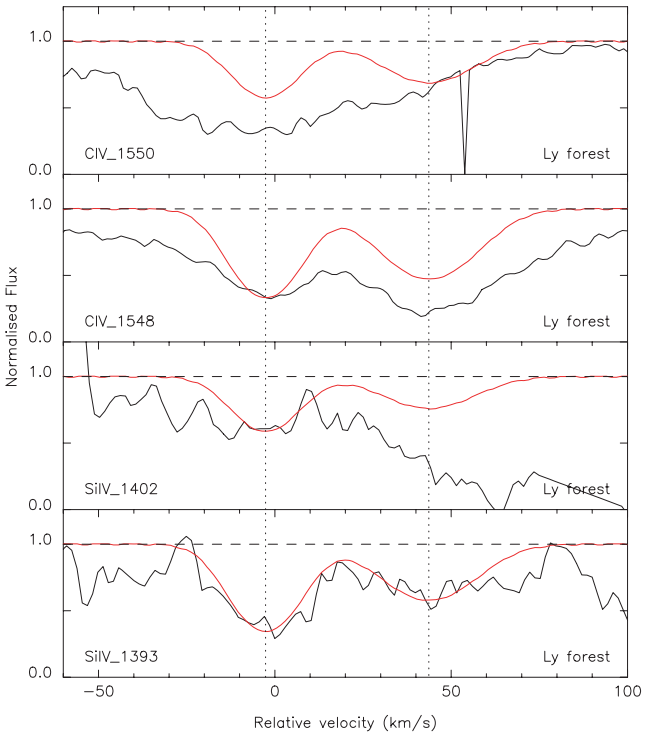

Figure 4. Fit to the high-ionization transitions of the $z_{abs} = 2.976$, $\log N(\mathrm{H\,I}) = 19.53 \pm 0.10$ sub-DLA towards PSS J0121+0347 (see Table 5).

Table 5. Parameters fitted to the high-ionization transitions of the $z_{abs} = 2.976$, $\log N(\mathrm{H\,I}) = 19.53 \pm 0.10$ sub-DLA towards PSS J0121+0347.

z	b	$\log N$(C IV)	$\log N$(Si IV)
2.975965	11.90 ± 0.08	<13.50	13.10 ± 0.10
2.976579	16.90 ± 0.08	<13.47	12.95 ± 0.10

$b > 100$ km s^{-1} single-component line. The strength of the two C IV lines of the doublet are consistent with their respective oscillator strengths, but they do not display the characteristic complex profiles of sub-DLA/DLAs. Therefore, care should be taken in interpreting these features as C IV. The column density derived is N(C IV) = 13.92 ± 0.11, but this system might be a large-N(H I) system with no C IV detected. This is illustrated in Fig. 8.

(v) **PSS J0133+0400** ($z_{em} = 4.154$, $z_{abs} = 3.139$, $\log N(\mathrm{H\,I}) = 19.01 \pm 0.10$)

This sub-DLA has a low $N_{\mathrm{H\,I}}$ column density, with $\log N(\mathrm{H\,I}) = 19.01 \pm 0.10$ at $z_{abs} = 3.139$. Unfortunately, many of the expected strong metal lines for this system fall in spectral gaps (i.e. Fe II λ1608, C IV $\lambda\lambda$1548, 1550) or are blended with H I lines from the Lyman α forest (i.e. the other Fe II λ lines). The two-component fit is performed on Si II λ1260 with a consistency check on Si II λ1808 to derive an upper limit on the total Si II column density. Attempts to increase the number of components do not improve the χ^2 of the fit

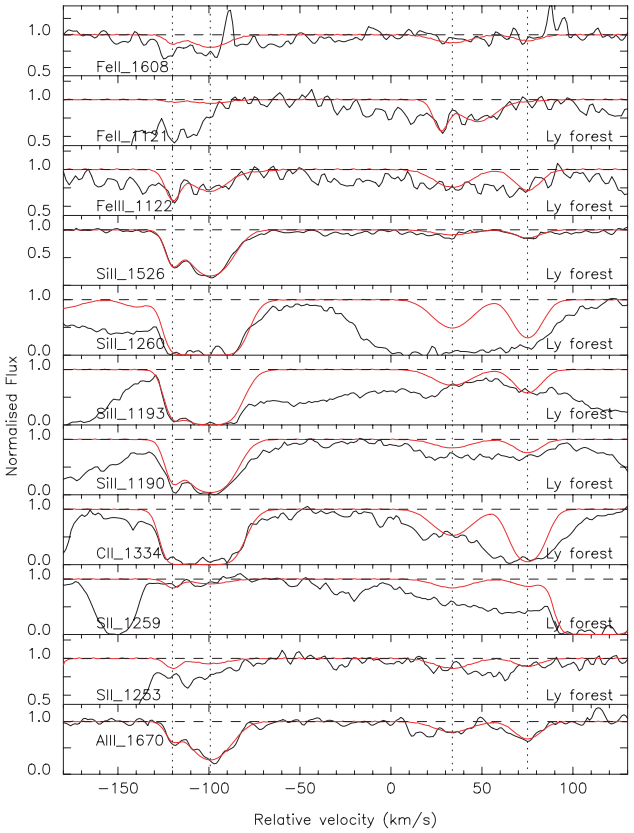

Figure 5. Fit to the low-ionization transitions of the $z_{abs} = 2.988$, $\log N(\mathrm{H\,I}) = 19.18 \pm 0.10$ sub-DLA towards SDSS J0124+0044 (see Table 6).

in this case. The same redshifts and b are applied to the blended C II λ1334 to derive an upper limit on the C abundance. The fit is shown in Fig. 9, and the matching parameters are presented in Table 9. Al III λ1854 is strongly blended, but Al III λ1862 is used to derive a 4σ upper limit: $\log N(\mathrm{Al\,III}) < 11.44$.

The position of the high-ionization transitions are unfortunate in this system too. Si IV λ1402 falls in a DLA along the same sight of line, and Si IV λ1393 is completely blended with H I lines from the Lyman α forest. The C IV doublet is situated in one of the spectral gaps of our data.

(vi) **PSS J0133+0400** ($z_{em} = 4.154$, $z_{abs} = 3.995$, $\log N(\mathrm{H\,I}) = 19.94 \pm 0.15$)

This system has a fairly high N(H I), with $\log N(\mathrm{H\,I}) = 19.94 \pm 0.15$ at $z_{abs} = 3.995$. The redshifts and values of b of the five components are derived from partially blended lines of Si II λ1260 (telluric contamination) for the two bluest components and of Si II λ1190 (Lyman α forest contamination) for the three remaining components. The resulting fit is checked on other Si II lines (Si II $\lambda\lambda$1193, 1260 and 1808). As a result, we can obtain an accurate value for the total N(Si II). Most of the Fe II λ lines in this system are blended with Lyman α forest features (Fe II $\lambda\lambda$1063, 1096, 1121 and 1125)

Table 6. Parameters fitted to the low-ionization transitions of the $z_{abs} = 2.988$, log N(H I) $= 19.18 \pm 0.10$ sub-DLA towards SDSS J0124+0044.

z	b	log N(Fe II)	log N(Si II)	log N(C II)	log N(S II)	log N(Al III)	log N(Fe III)
2.986404	2.90 ± 0.01	<12.62	13.41 ± 0.13	<15.67	<13.48	11.68 ± 0.16	<13.39
2.986680	12.50 ± 0.61	<13.20	13.98 ± 0.11	<14.62	<13.59	12.58 ± 0.12	<13.59
2.988448	12.80 ± 0.03	<13.00	12.71 ± 0.16	<13.53	<13.88	11.82 ± 0.13	<13.51
2.988998	8.50 ± 0.20	<12.72	12.78 ± 0.16	<14.07	<13.63	11.93 ± 0.14	<13.44

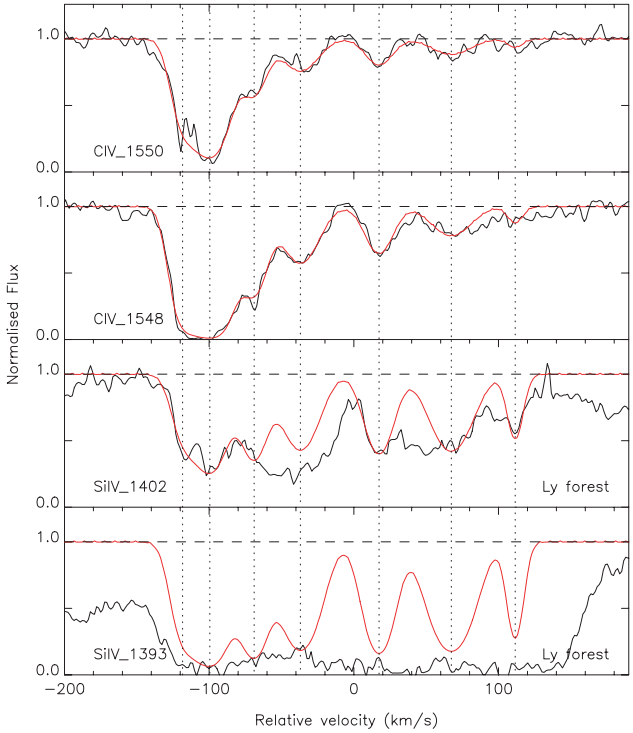

Figure 6. fit to the high-ionization transitions of the $z_{abs} = 2.988$, log N(HI) $= 19.18 \pm 0.10$ sub-DLA towards SDSS J0124+0044 (Table 7).

Table 7. Parameters fitted to the high-ionization transitions of the $z_{abs} = 2.988$, log N(H I) $= 19.18 \pm 0.10$ sub-DLA towards SDSS J0124+0044.

z	b	log N(C IV)	log N(Si IV)
2.986426	9.40 ± 0.01	13.60 ± 0.02	<13.00
2.986677	14.70 ± 0.61	14.19 ± 0.18	<13.59
2.987084	10.70 ± 0.03	13.44 ± 0.02	<13.34
2.987509	15.60 ± 0.02	13.31 ± 0.08	<13.41
2.988232	11.94 ± 0.10	13.10 ± 1.04	<13.34
2.988896	17.70 ± 0.05	13.01 ± 0.07	<13.47
2.989483	5.70 ± 0.05	12.33 ± 1.41	<12.97

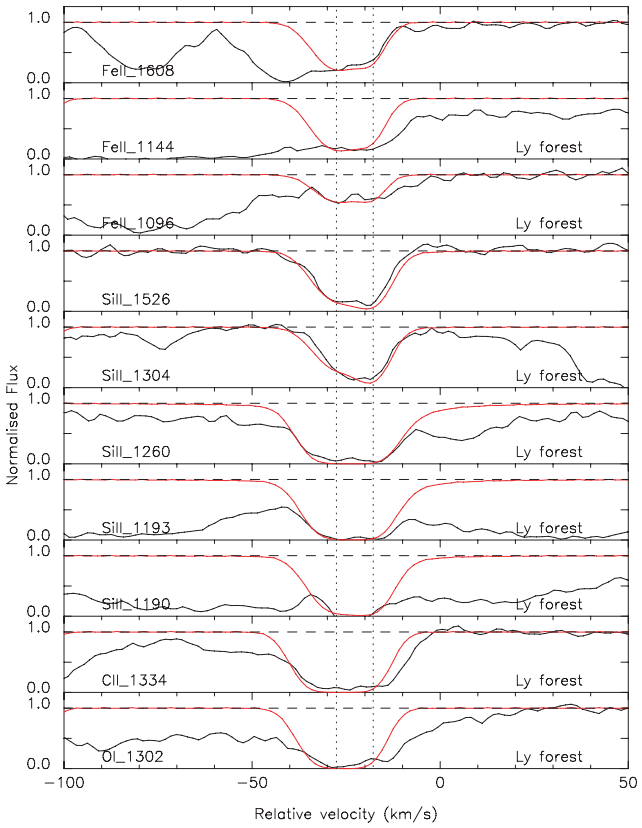

Figure 7. Fit to the low-ionization transitions of the $z_{abs} = 3.078$, log N(HI) $= 20.21 \pm 0.10$ sub-DLA towards SDSS J0124+0044 (see Table 8).

Table 8. Parameters fitted to the low-ionization transitions of the $z_{abs} = 3.078$, log N(H I) $= 20.21 \pm 0.10$ sub-DLA towards SDSS J0124+0044.

z	b	log N(Fe II)	log N(Si II)	log N(C II)	log N(O I)
3.077625	6.20 ± 3.20	<13.95	13.75 ± 0.20	>14.93	>15.00
3.077758	2.10 ± 0.40	<13.65	15.11 ± 0.40	>15.15	>14.60

or fall in a zero-flux gap (Fe II λλ1143 and 1144) owing to DLAs along the same line of sight. Only the Fe II λ1608 line is covered by our spectrum, but it is undetected. We derive an upper limit of log N(Fe II) < 13.56 at 4σ. Other ions are not detected and allow the derivation of upper limits: log N(Ni II) < 12.31, log N(Al II) < 11.36, and log N(Al III) < 11.69. The fit is shown in Fig. 10, and the matching parameters are presented in Table 10.

The five components for the high-ionization transitions are derived from a simultaneous fit of the lines Si IV λλ1393 and 1402. Si IV λ1393 provides a column density determination free from any contamination. The same redshifts and values of b are used to fit the C IV doublet of the system and to derive an upper limit on this blended line. The fit is shown in Fig. 11, and the matching parameters are presented in Table 11.

(vii) **PSS J0133+0400** ($z_{em} = 4.154$, $z_{abs} = 3.999$, log N(HI) $= 19.16 \pm 0.15$)

This system is at the low end of the column-density distribution for sub-DLAs, with log N(H I) $= 19.16 \pm 0.15$ at $z_{abs} = 3.999$. Most Si III lines are covered in this absorber, but many are blended with Lyman α forest contamination (i.e. Si II λλ 1190, 1193) or telluric

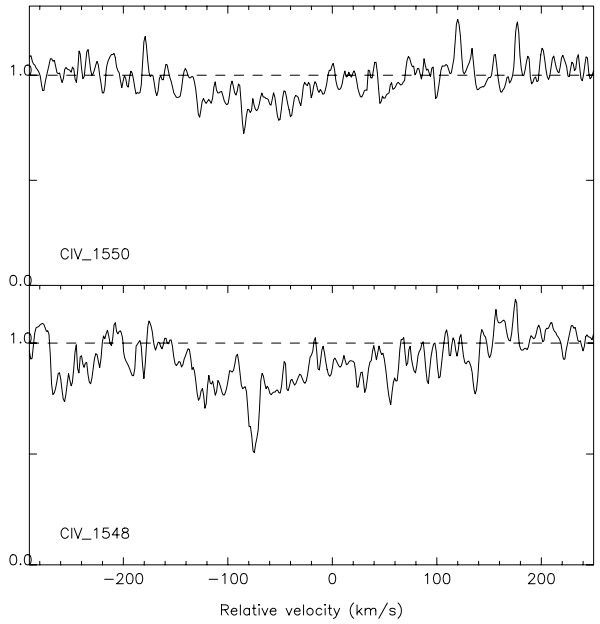

Figure 8. High-ionization ions of the absorber detected towards SDSS J0124+0044 with $\log N(\mathrm{H\,I}) = 20.21 \pm 0.10$ at $z_{\rm abs} = 3.078$.

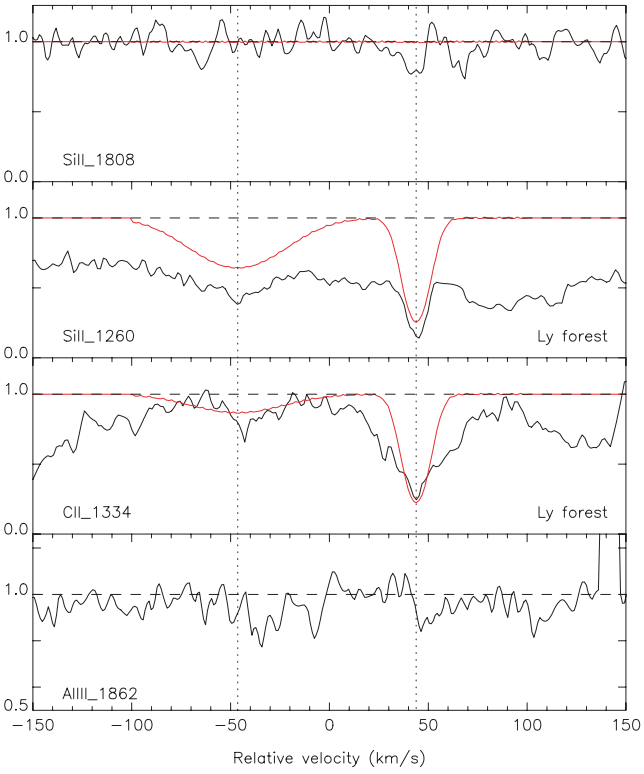

Figure 9. Fit to the low-ionization transitions of the $z_{\rm abs} = 3.139$, $\log N(\mathrm{H\,I}) = 19.01 \pm 0.10$ sub-DLA towards PSS J0133+0400 (see Table 9). The fit of C II λ1334 is used to derive an upper limit on the C II column density.

contamination (Si II λλ1260, 1526). Si II λ1304 falls in a spectral gap. Therefore, the region around the expected position for Si II λ1808 is used to derive an upper limit on the abundance of Si III: $\log N(\mathrm{Si\,II}) < 14.12$ at 4σ. Similarly, upper limits are derived for non-detection as follows: $\log N(\mathrm{Al\,II}) < 11.10$ from Al II λ1670; $\log N(\mathrm{Al\,III}) < 11.63$ from Al III λ1854; and $\log N(\mathrm{Fe\,II}) < 13.56$ from Fe II λ1608.

Table 9. Parameters fitted to the low-ionization transitions of the $z_{\rm abs} = 3.139$, $\log N(\mathrm{H\,I}) = 19.01 \pm 0.10$ sub-DLA towards PSS J0133+0400.

z	b	$\log N$(Si II)	$\log N$(C II)
3.138360	31.60 ± 0.20	<12.87	<13.25
3.139605	7.40 ± 0.10	<12.81	<13.72

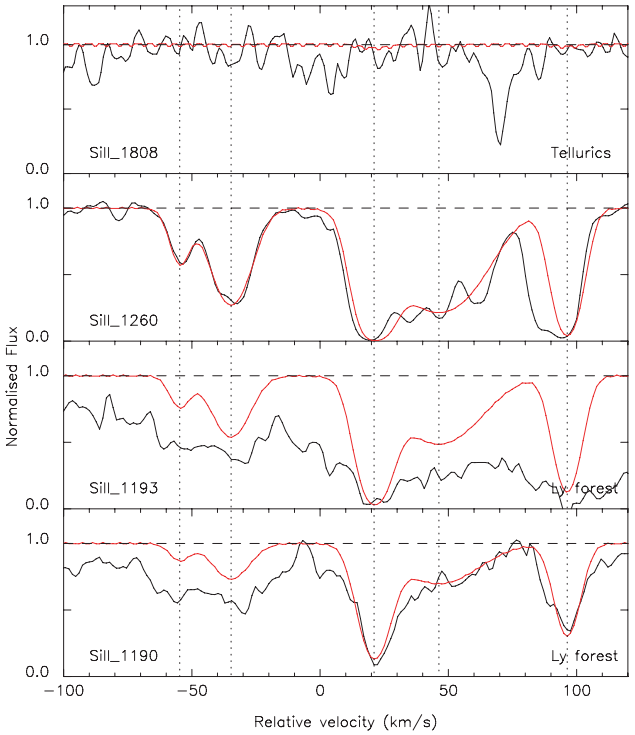

Figure 10. Fit to the low-ionization transitions of the $z_{\rm abs} = 3.995$, $\log N(\mathrm{H\,I}) = 19.94 \pm 0.15$ sub-DLA towards PSS J0133+0400 (see Table 10).

Table 10. Parameters fitted to the low-ionization transitions of the $z_{\rm abs} = 3.995$, $\log N(\mathrm{H\,I}) = 19.94 \pm 0.15$ sub-DLA towards PSS J0133+0400.

z	b	$\log N$(Si II)
3.994089	3.10 ± 0.16	12.24 ± 0.12
3.994422	8.50 ± 0.11	12.83 ± 0.11
3.995350	5.90 ± 0.21	13.56 ± 0.14
3.995771	20.00 ± 0.15	13.22 ± 0.11
3.996604	4.70 ± 0.11	13.29 ± 0.18

For the high-ionization transitions, a fit is performed on C IV λλ1548 and 1550 simultaneously. The same redshifts and values of b are used for the Si IV λ1393/1402 doublet. All these lines appear broad and noisy, and therefore lead to upper limits. The fit is shown in Fig. 12, and the matching parameters are presented in Table 12.

(viii) **PSS J0133+0400** ($z_{\rm em} = 4.154$, $z_{\rm abs} = 4.021$, $\log N(\mathrm{H\,I}) = 19.09 \pm 0.15$)

This is also a system at the low end of the column-density range of sub-DLAs, with $\log N(\mathrm{H\,I}) = 19.09 \pm 0.15$ at $z_{\rm abs} = 4.021$. Again, many lines for this absorber are blended in the Lyman α forest. Upper limits from non-detections of Al II λ1670, Si II λ1808

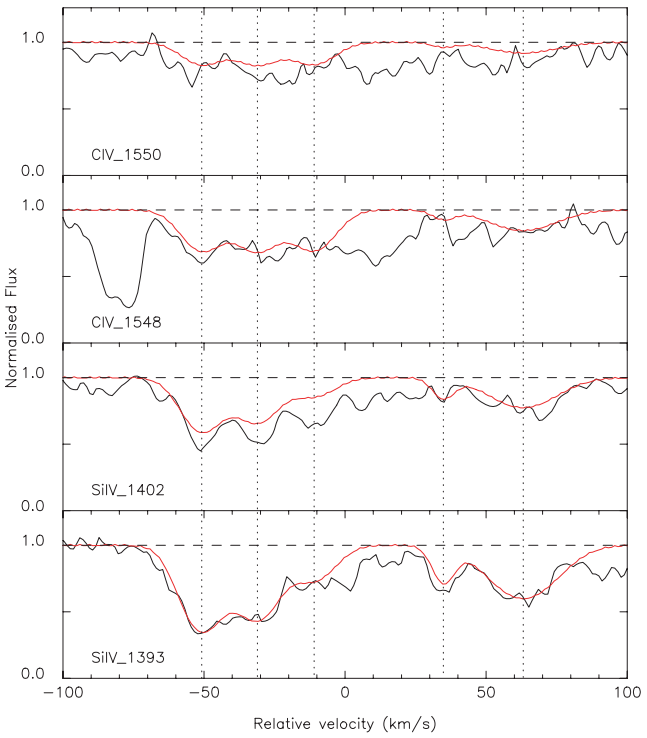

Figure 11. Fit to the high-ionization transitions of the $z_{\rm abs} = 3.995$, $\log N({\rm H\,I}) = 19.94 \pm 0.15$ sub-DLA towards PSS J0133+0400 (see Table 11).

Table 11. Parameters fitted to the high-ionization transitions of the $z_{\rm abs} = 3.995$, $\log N({\rm H\,I}) = 19.94 \pm 0.15$ sub-DLA towards PSS J0133+0400.

z	b	$\log N$(C IV)	$\log N$(Si IV)
3.994154	8.90 ± 0.01	<12.92	12.99 ± 0.25
3.994482	9.30 ± 0.86	<12.94	12.90 ± 0.03
3.994817	9.30 ± 0.03	<12.93	12.47 ± 0.49
3.995580	3.20 ± 0.92	<11.95	12.24 ± 0.42
3.996051	15.60 ± 1.33	<12.79	12.89 ± 0.01

and Fe II λ1608 are derived at the 4σ level: $\log N({\rm Al\,II}) < 11.20$, $\log N({\rm Si\,II}) < 14.05$, and $\log N({\rm Fe\,II}) < 13.56$.

A kinematically simple broad absorption is detected at the position of the Si IV doublet. The profiles are fitted using both lines simultaneously to derive an upper limit. The C IV doublet, however, is not detected in this system. An upper limit on the abundance is derived to be $\log N({\rm C\,IV}) < 12.31$. The fit is shown in Fig. 13, and the matching parameters are presented in Table 13.

(ix) **BRI J0137−4224** ($z_{\rm em} = 3.970$, $z_{\rm abs} = 3.101$, $\log N({\rm H\,I}) = 19.81 \pm 0.10$)

The lower-redshift sub-DLA of this quasar has many metal lines falling in the Lyman α forest. With a column density of $\log N({\rm H\,I}) = 19.81 \pm 0.10$ at $z_{\rm abs} = 3.101$, it is situated in the mid-range of the sub-DLA definition. Nevertheless, some strong lines are undoubtably clear from any contamination. Si II λ1526 and Al II λ1670 in particular are used to derive the redshifts and values of b of the seven components used to fit the metal-line profile. The resulting values of z and b are used to derive the abundance of Fe II from a fit to the Fe II λ1608 line. The remaining Fe II λ lines (i.e. Fe II $\lambda\lambda$1096, 1144) are heavily blended with Lyman α forest contamination. The fit is shown in Fig. 14, and the matching parameters are presented in Table 14.

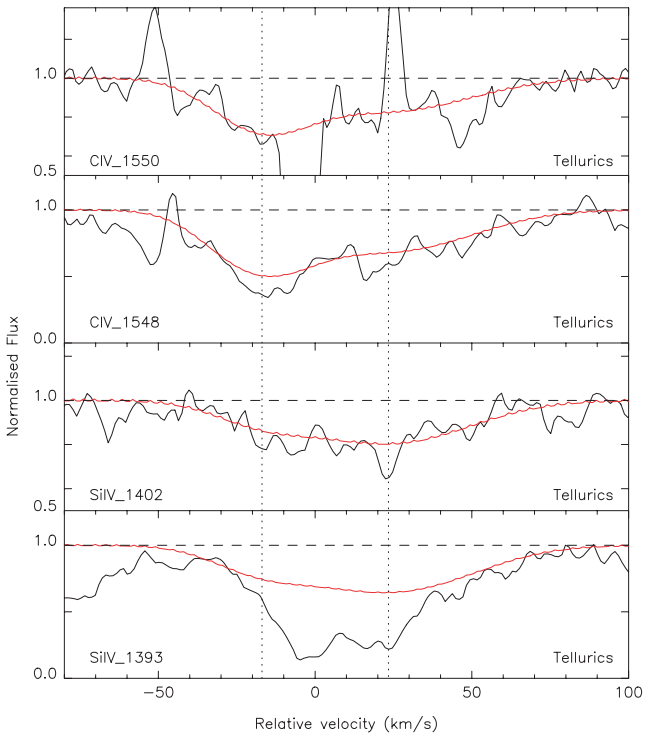

Figure 12. Fit to the high-ionization transitions of the $z_{\rm abs} = 3.999$, $\log N({\rm H\,I}) = 19.16 \pm 0.15$ sub-DLA towards PSS J0133+0400 (see Table 12).

Table 12. Parameters fitted to the high-ionization transitions of the $z_{\rm abs} = 3.999$, $\log N({\rm H\,I}) = 19.16 \pm 0.15$ sub-DLA towards PSS J0133+0400.

z	b	$\log N$(C IV)	$\log N$(Si IV)
3.998718	20.40 ± 0.40	<13.44	<12.55
3.999390	34.60 ± 0.30	<13.47	<13.15

Table 13. Parameters fitted to the high-ionization transitions of the $z_{\rm abs} = 4.021$, $\log N({\rm H\,I}) = 19.09 \pm 0.15$ sub-DLA towards PSS J0133+0400.

z	b	$\log N$(Si IV)
4.021325	30.3 ± 1.00	<12.89

Concerning the high-ionization transitions, the Si IV doublet falls in the Lyman α forest, and is therefore totally blended and not useful for abundance determination. Similarly, the C IV doublet is blended with unidentified lines as well as with apparent emission lines, which are probably the products of bad cosmic-ray clipping (no telluric lines were identified in this region) and are removed to perform the fit. The C IV λ1550 is fitted with eight components, and the resulting profile is made consistent with C IV λ1548. The fit is shown in Fig. 15, and the matching parameters are presented in Table 15.

(x) **BRI J0137−4224** ($z_{\rm em} = 3.970$, $z_{\rm abs} = 3.665$, $\log N({\rm H\,I}) = 19.11 \pm 0.10$)

This sub-DLA has a fairly low column density of $\log N({\rm H\,I}) = 19.11 \pm 0.10$ at $z_{\rm abs} = 3.665$. Nevertheless, it shows strong, kinematically simple, metal lines, which are well fitted by a single

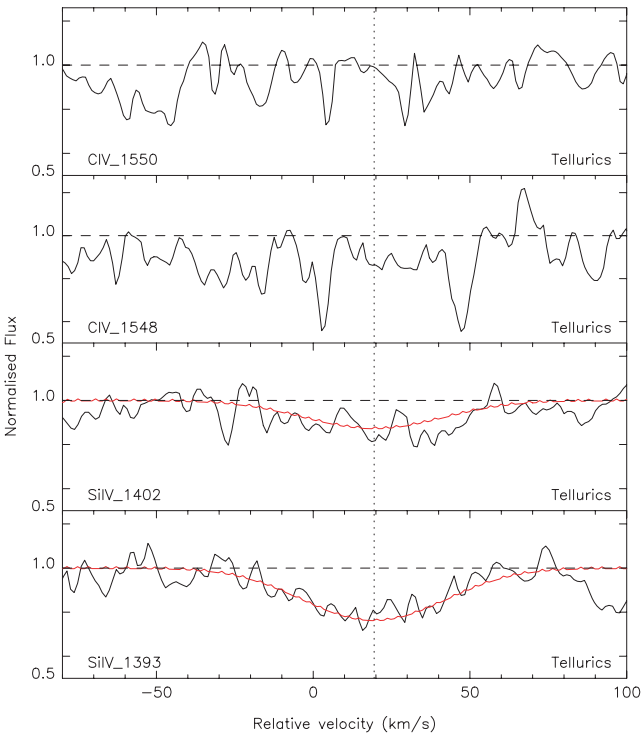

Figure 13. Fit to the high-ionization transitions of the $z_{abs} = 4.021$, $\log N(\mathrm{I}) = 19.09 \pm 0.15$ sub-DLA towards PSS J0133+0400 (see Table 13).

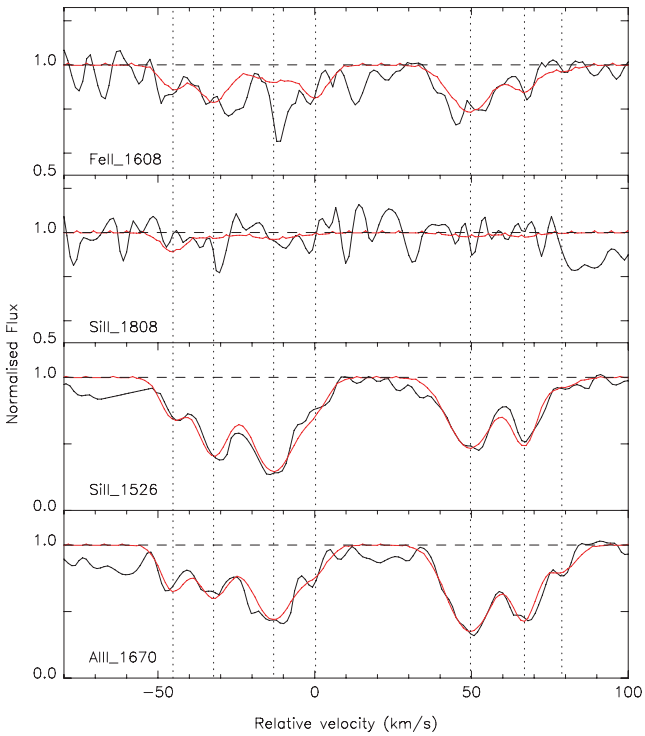

Figure 14. Fit to the low-ionization transitions of the $z_{abs} = 3.101$, $\log N(\mathrm{HI}) = 19.81 \pm 0.10$ sub-DLA towards BRI J0137−4224 (see Table 14).

component. Three lines (O I λ1302, Si II λ1260 and C II λ1334) that are clear from any contamination are fitted simultaneously to derive the redshift, b and appropriate column densities. The resulting fit is overplotted on the many blended Si III lines (Si II λλ1304, 1190, 1190, 1526 and 1808) and is found to be consistent in all cases. Unfortunately, many of the Fe II λ lines for the system fall in regions contaminated by Lyman α forest lines (Fe II λλ1063, 1096, 1121, 1125, 1143 and 1144). Only Fe II λ1608 lies in a region free from any contamination, but the signal-to-noise ratio of the spectrum is low. This leads to an upper limit of $\log N(\mathrm{Fe\,II}) < 13.59$ at 4σ. Al II λ1670 and Al III λ1854/Al III λ1862 are covered by our spectrum but no lines are detected. Upper limits on the column densities of these ions are derived as: $\log N(\mathrm{Al\,II}) < 11.06$ and $\log N(\mathrm{Al\,III}) < 11.96$. The fit is shown in Fig. 16, and the matching parameters are presented in Table 16.

The high-ionization transitions of this system present a very particular signature. Both lines of the Si IV doublet (1393 and 1402) are clearly detected and very well fitted by a simple two-component profile. Rather surprisingly, however, both C IV lines (1548 and 1550) of the C IV doublet are covered by our data but *seem* to be undetected. In fact, the weak component falling at the expected redshift in C IV λ1550 happens to be a telluric line, although the C IV λ1548 region is free from telluric contamination. At any rate, this line is within the noise of the spectrum and cannot definitely be assumed to be a real line. From the signal-to-noise ratio in the region where the doublet is expected to fall, we deduce an upper limit on the column density of $\log N(\mathrm{C\,IV}) < 12.11$ at 4σ. Interestingly, in Dessauges-Zavadsky et al. (2003), we reported the detection in a sub-DLA of C IV lines with no associated Si IV. However, to our knowledge this is the first time that a large N_{HI} absorber has been reported to have Si IV but no C IV detected. This could be a signature of Si IV associated with the N_{HI} gas, with C IV part of an external shell surrounding the region. The fit is shown in Fig. 17, and the matching parameters are presented in Table 17.

Table 14. Parameters fitted to the low-ionization transitions of the $z_{abs} = 3.101$, $\log N(\mathrm{H\,I}) = 19.81 \pm 0.10$ sub-DLA towards BRI J0137−4224.

z	b	$\log N$(Fe II)	$\log N$(Si II)	$\log N$(Al III)
3.100382	2.90 ± 2.64	12.65 ± 0.39	12.92 ± 0.33	11.73 ± 0.14
3.100559	4.90 ± 0.11	12.95 ± 0.01	13.40 ± 0.20	11.88 ± 0.89
3.100821	7.40 ± 0.91	12.70 ± 0.01	13.64 ± 0.29	12.20 ± 0.72
3.101004	3.30 ± 0.12	12.80 ± 0.12	12.73 ± 0.22	11.40 ± 0.54
3.101679	8.00 ± 0.77	13.20 ± 0.01	13.45 ± 0.25	12.33 ± 0.49
3.101915	3.20 ± 0.22	12.70 ± 0.01	13.25 ± 0.10	12.06 ± 0.10
3.102078	4.10 ± 0.40	12.10 ± 0.01	12.27 ± 0.20	11.48 ± 0.20

(xi) **BR J2215−1611** ($z_{em} = 3.990$, $z_{abs} = 3.656$, $\log N(\mathrm{H\,I}) = 19.01 \pm 0.15$)

The two sub-DLAs detected towards BR J2215−1611 are essentially blended together and are only separated at the Lyman-γ level. The first system, at $z_{abs} = 3.656$, has the weakest H I column density, with $\log N(\mathrm{H\,I}) = 19.01 \pm 0.15$. Metal lines are seldom detected, partly because of contamination with the Lyman α forest lines. A few lines (Si II λλ1304, 1526, 1808 and Fe II λ1608) fall in regions free from any contamination and yet remain undetected. We derive upper limits on the column densities of the corresponding ions: $\log N(\mathrm{Si\,II}) < 14.41$, $\log N(\mathrm{Fe\,II}) < 13.51$, and $\log N(\mathrm{S\,II}) < 13.68$. The intermediate ionization transitions Al III λλ1854 and 1862 fall in the region polluted by telluric lines, which prevents us from any detection or determination of an upper limit.

The high-ionization transitions C IV λλ1548 and 1550 are detected in this system. To the immediate blue wavelength of the C IV λ1548 line lies a telluric line. The profile is well fitted by one component

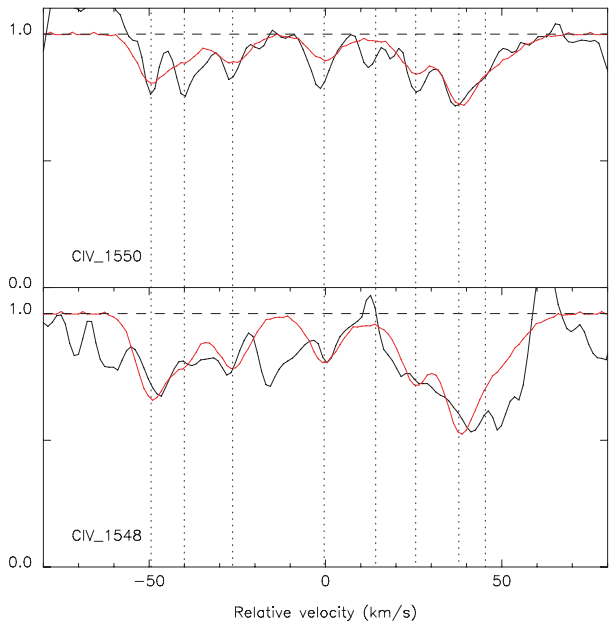

Figure 15. Fit to the high-ionization transitions of the $z_{abs} = 3.101$, log N(HI) = 19.81 ± 0.10 sub-DLA towards BRI J0137−4224 (see Table 15).

Table 15. Parameters fitted to the high-ionization transitions of the $z_{abs} = 3.101$, log N(H I) = 19.81 ± 0.10 sub-DLA towards BRI J0137−4224.

z	b	log N(C IV)
3.100324	3.50 ± 0.16	12.74 ± 0.18
3.100453	3.20 ± 0.07	12.43 ± 0.10
3.100640	4.50 ± 0.28	12.55 ± 0.14
3.100995	3.10 ± 0.24	12.38 ± 0.10
3.101195	20.40 ± 0.12	12.34 ± 0.34
3.101350	3.20 ± 0.23	12.57 ± 0.10
3.101517	3.20 ± 0.10	12.79 ± 0.25
3.101620	9.90 ± 0.20	12.83 ± 0.13

whose characteristics are derived from a simultaneous fit of the two members of the doublet, but, to be conservative, only an upper limit is derived. The Si IV in this sub-DLA is not detected, although both lines of the doublet are covered by our data. This leads to an upper limit on the column density: log N(Si IV) < 11.69. The fit is shown in Fig. 18, and the matching parameters are presented in Table 18.

(xii) **BR J2215−1611** ($z_{em} = 3.990$, $z_{abs} = 3.662$, log N(H I) = 20.05 ± 0.15)

In contrast to the previous system, this sub-DLA has a fairly high N(H I) column density of log N(H I) = 20.05 ± 0.15 at $z_{abs} = 3.662$. It is characterized by strong metal lines showing a complex profile over ∼100 km s^{-1}. The five components are simultaneously fitted to O I λ1302, the unsaturated components, C II λ1334, Al II λ1670, and Si II λ1526. The first component is narrower in Si II λ1526 than in the other metal lines, including Si II λ1304. We note, however, that O I λ1302 is controversial, and that it is a borderline case between a lower limit and a value.

The resulting fit is applied to the other Si II lines: Si II λ1304 is clearly well fitted by this profile; Si II λ1808 is not detected, in agreement with our fit; and Si II λλ1190, 1193 and 1260, which are situated in the Lyman α forest, are clearly blended by other intervening lines. Nevertheless, the fit is found to be consistent with

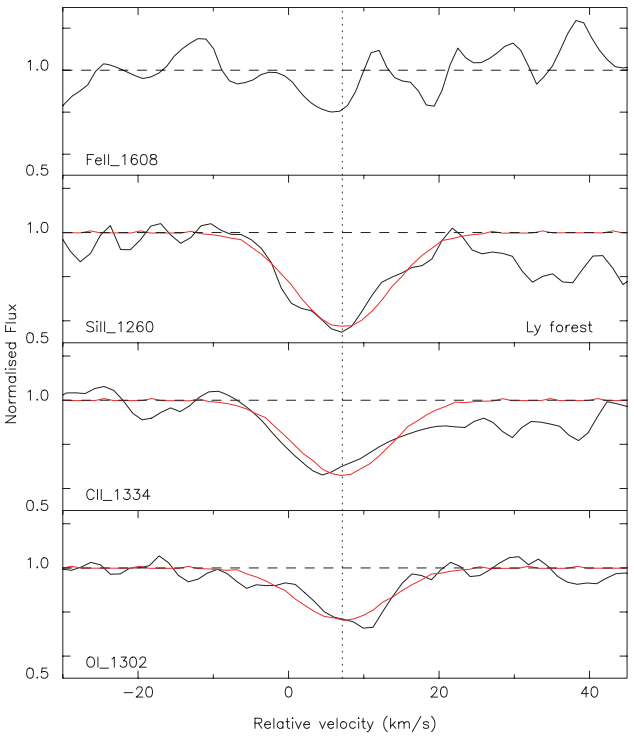

Figure 16. Fit to the low-ionization transitions of the $z_{abs} = 3.665$, log N(H I) = 19.11 ± 0.10 sub-DLA towards BRI J0137−4224 (see Table 16). The region 25–45 km s^{-1} is contaminated by an unidentified blend.

Table 16. Parameters fitted to the low-ionization transitions of the $z_{abs} = 3.665$, log N(H I) = 19.11 ± 0.10 sub-DLA towards BRI J0137−4224.

z	b	log N(Si II)	log N(C II)	log N(O I)
3.665111	7.02 ± 0.50	12.40 ± 0.13	13.14 ± 0.13	13.38 ± 0.13

the upper limit they provide. All Fe II λ lines except Fe II λ1125 are contaminated, but we use the non-detection of Fe II λ1125 to derive log N(Fe II)<13.60. The fit is shown in Fig. 19, and the matching parameters are presented in Table 19. The intermediate ionization transitions Al III λλ1854 and 1862 fall in the region polluted by telluric lines, which prevents us from any detection or determination of an upper limit.

The high-ionization transitions in this system are well fitted with three components. The redshifts and values of b of these are determined by a simultaneous fit of the C IV λ 1548 and Si IV λ1402 lines. The fit is then superimposed on C IV λ1550 and Si IV λ1393. Clearly, the Si IV λ1393 line is blended, although no telluric lines are seen in this region. This fit leads to accurate column-density determinations. The fit is shown in Fig. 20, and the matching parameters are presented in Table 20.

(xiii) **BR J2216−6714** ($z_{em} = 4.469$, $z_{abs} = 3.368$, log N(H I) = 19.80 ± 0.10)

This sub-DLA has a mid-range column density of log N(H I) = 19.80 ± 0.10 at $z_{abs} = 3.368$. However, the low-ionization transitions in this system are barely detected, partly because of Lyman α contamination (the metal lines with λ_{rest} <1522 Å in this sub-DLA fall in the forest). This applies to many of the Si II lines (Si II λλ1304, 1260, 1193, 1190 and 1526). The non-detection of Si II λ1808 leads to the determination of an upper limit: log N(Si II) < 13.88 at 4σ. Similarly, most of the Fe II lines are in the forest, but the region at the

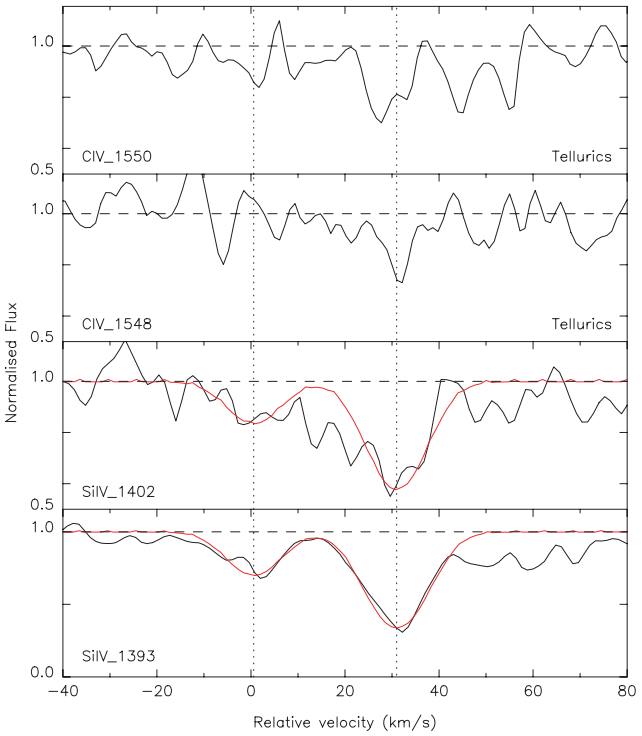

Figure 17. Fit to the high-ionization transitions of the $z_{\rm abs} = 3.665$, $\log N({\rm H\,I}) = 19.11 \pm 0.10$ sub-DLA towards BRI J0137−4224 (see Table 17).

Table 17. Parameters fitted to the high-ionization transitions of the $z_{\rm abs} = 3.665$, $\log N({\rm H\,I}) = 19.11 \pm 0.10$ sub-DLA towards BRI J0137−4224.

z	b	$\log N$(Si IV)
3.665009	6.60 ± 5.20	12.43 ± 0.22
3.665482	7.30 ± 3.80	12.95 ± 0.10

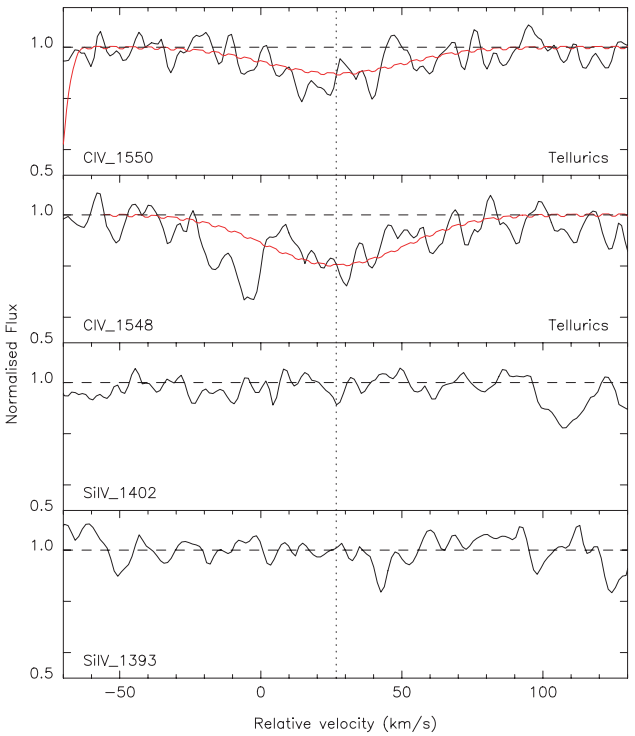

Figure 18. Fit to the high-ionization transitions of the $z_{\rm abs} = 3.656$, $\log N({\rm H\,I}) = 19.01 \pm 0.15$ sub-DLA towards BR J2215−1611 (see Table 18).

Table 18. Parameters fitted to the high-ionization transitions of the $z_{\rm abs} = 3.656$, $\log N({\rm H\,I}) = 19.01 \pm 0.15$ sub-DLA towards BR J2215−1611.

z	b	$\log N$(C IV)
3.656415	33.30 ± 16.86	<13.22

expected position of Fe II λ1608 has a fairly high signal-to-noise ratio, leading to a constraining upper limit on the Fe II column density: $\log N({\rm Fe\,II}) < 13.26$. Al III λλ1854 and 1862 are also undetected: $\log N({\rm Al\,III}) < 11.51$. On the other hand, a two-component feature at the expected position of Al II λ1670 is clearly detected. We compute an abundance determination for this element. The fit is shown in Fig. 21, and the matching parameters are presented in Table 21.

In addition, high-ionization transitions are detected for this system. The C IV doublet is clearly detected and leads to an accurate column-density determination using a simultaneous fit of both members of the doublet to determine the redshifts and values of b of six components. The Si IV doublet appears to be blended with Lyman α forest interlopers, although Si IV λ1393 is probably free from any contamination. The parameters derived from C IV are used to determine the upper limits on Si IV λ1393, but the first and fourth components are not detected in Si IV. The fit is shown in Fig. 22, and the matching parameters are presented in Table 22.

3 RESULTS

3.1 Individual abundances

The resulting total column densities for each of the elements detected in the 13 sub-DLAs studied here are summarized in Table 23, together with the error estimates.

One concern is that sub-DLAs may be partially ionized in H, in which case the observed Fe II to H I ratio would not be a good measure of the total Fe abundance, for instance. Indeed, given that Fe II has an ionization potential, IP(Fe II) = 16.18 eV, larger than hydrogen, IP(H I) = 13.59 eV, some of the observed Fe II could reside in the ionized gas of the sub-DLA with lower $N({\rm H\,I})$. This leads to a slight overestimate of the true total metallicity of the systems. To investigate the ionization corrections, we compute photoionization models based on the CLOUDY software package (version 94.00, Ferland 1997), assuming ionization equilibrium and a solar abundance pattern. Based on the modelling of 13 systems, Dessauges-Zavadsky et al. (2003) have shown that differences between a Haardt–Madau or a stellar-like spectrum are negligible. Here, we chose to perform the modelling using a stellar-like incident ionization spectrum (D'Odorico & Petitjean 2001). We thus obtain the theoretical column-density predictions for any ionization state of all observed ions as a function of the ionization parameter U. When possible, we then use observed ratios of the same element in different states (i.e. Fe II/Fe III, Al II/Al III, Si III/Si IV or C II/C IV) and compare them with predictions from the model to constrain the U parameter. When only limits on the U parameter are available, we established a limit on the ionization correction. On two occasions, such ratios are not available and the observed column densities are directly compared with the predicted ones to deduce the U parameter.

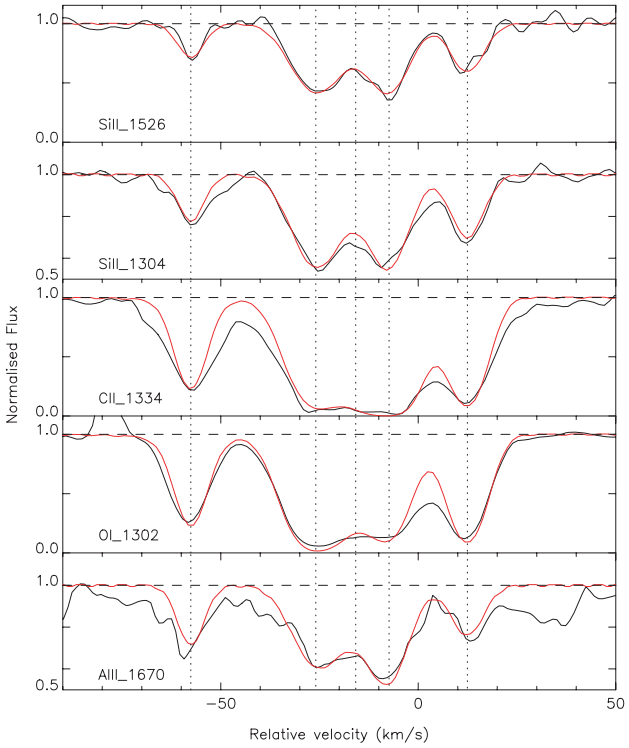

Figure 19. Fit to the low-ionization transitions of the $z_{\rm abs} = 3.662$, $\log {\rm N(H\,I)} = 20.05 \pm 0.15$ sub-DLA towards BR J2215−1611 (see Table 19).

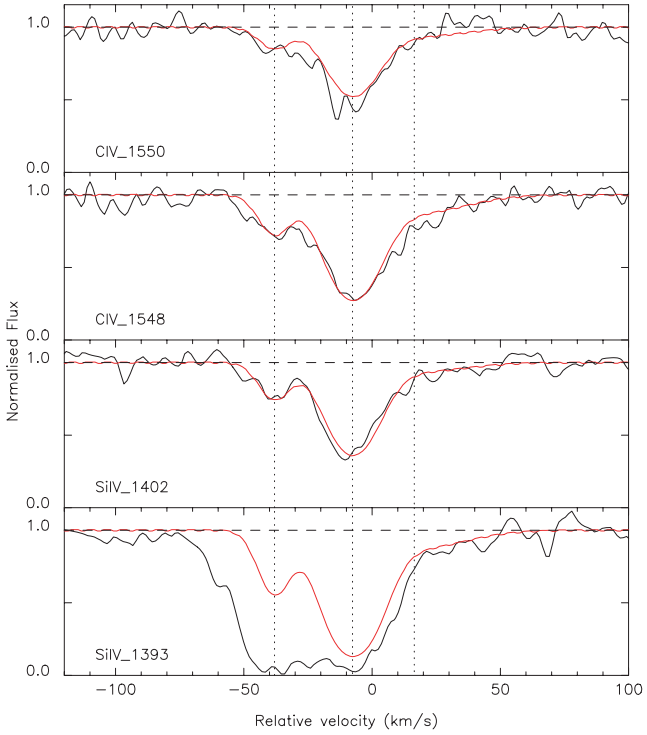

Figure 20. Fit to the high-ionization transitions of the $z_{\rm abs} = 3.662$, $\log {\rm N(I)} = 20.05 \pm 0.15$ sub-DLA towards BR J2215−1611 (see Table 20).

Once the ionization parameter U is known, we can deduce by how much the observed metallicity, Fe II$_{\rm obs}$/H I$_{\rm obs}$, deviates from the total metallicity, Fe$_{\rm TOT}$/H $_{\rm TOT}$, of the absorber. We compute the correction to apply to the observed Fe II values, the so-called $\delta_{\rm ioni}$, as follows:

$$\delta_{\rm ioni} = \frac{\rm Fe_{TOT}}{\rm H_{TOT}} - \frac{\rm Fe\,II_{obs}}{\rm H\,I_{obs}}. \quad (1)$$

A negative (positive) $\delta_{\rm ioni}$ corresponds to an overestimate (underestimate) of the total metallicity. Fig. 23 shows the corrections for 26 sub-DLAs as a function of N(H I) column densities from the present study and from the literature (Prochaska 1999; Dessauges-Zavadsky et al. 2003; Péroux et al. 2006a; Prochaska 2006). Recent findings by Fox et al. (2007) on the ionized fraction in O and C of a sample of DLAs are in line with the present results. The solid line is a fit to the measures (as opposed to lower limits) with slope $\alpha = 0.13$. As in Dessauges-Zavadsky et al. (2003) and more recently Prochaska et al. (2006), we find that the ionization corrections for sub-DLAs are small and within the error estimates in most cases (see also Erni et al. 2006, for a borderline case). In the present study, only four sub-DLAs out of the 13 studied require a correction $|\delta_{\rm ioni}| > 0.2$ dex. In all these four cases, the correction is $|\delta_{\rm ioni}| < 0.35$ dex. The $\delta_{\rm ioni}$ values for each sub-DLA are listed in Table 24. There is a hint of decreasing $\delta_{\rm ioni}$ with metallicity (Fig. 24). Knowing that sub-DLAs are more metal-rich than classical DLAs (Kulkarni et al. 2007), possibly owing to an observational bias, and that the ionization correction increases with decreasing $N_{\rm H\,I}$ (see Fig. 23), it is no surprise to observe that the ionization correction increases with the metallicity. It is interesting to note, though, that the fractional correction remains roughly constant. However, no clear correlation of $\delta_{\rm ioni}$ with absorption redshift is detected (Fig. 25), contrary to what one would expect from the redshift evolution of the incident UV background photons.

The total absolute abundances were calculated with respect to solar abundances using the following formula:

$$[X/H] = \log[N(X)/N(H)]_{\rm DLA} - \log[N(X)/N(H)]_{\odot}, \quad (2)$$

where $\log [N(X)/N(H)]_{\odot}$ is the solar abundance and is taken from Asplund et al. (2005) adopting the mean of photospheric and meteoritic values for Fe, Si, C, O, S and Al. These values are recalled on the top line of Table 24.

3.2 Global metallicity

Fig. 26 shows the resulting redshift evolution of the metallicity of DLAs and sub-DLAs, including our new sample of 13 high-redshift

Table 19. Parameters fitted to the low-ionization transitions of the $z_{\rm abs} = 3.662$, $\log N({\rm H\,I}) = 20.05 \pm 0.15$ sub-DLA towards BR J2215−1611.

z	b	$\log N$(Si II)	$\log N$(C II)	$\log N$(O I)	$\log N$(Al II)
3.661105	3.30 ± 0.10	12.95 ± 0.28	13.72 ± 0.48	14.03 ± 0.01	11.70 ± 0.16
3.661597	6.80 ± 0.10	13.45 ± 0.02	>13.95	14.61 ± 0.20	11.92 ± 0.27
3.661754	6.80 ± 0.20	12.60 ± 0.03	>13.35	13.61 ± 0.02	11.47 ± 0.10
3.661885	5.10 ± 0.10	13.38 ± 0.01	14.81 ± 0.20	14.25 ± 0.01	11.95 ± 0.67
3.662193	3.50 ± 0.10	13.11 ± 0.02	>14.16	14.58 ± 0.02	11.55 ± 0.53

Table 20. Parameters fitted to the high-ionization transitions of the $z_{abs} = 3.662$, log N(H I) $= 20.05 \pm 0.15$ sub-DLA towards BR J2215−1611.

z	b	log N(C IV)	log N(Si IV)
3.661409	7.20 ± 5.00	12.79 ± 0.07	12.67 ± 0.08
3.661881	12.40 ± 3.10	13.57 ± 0.25	13.39 ± 0.04
3.662255	26.50 ± 8.80	12.92 ± 0.08	12.53 ± 0.07

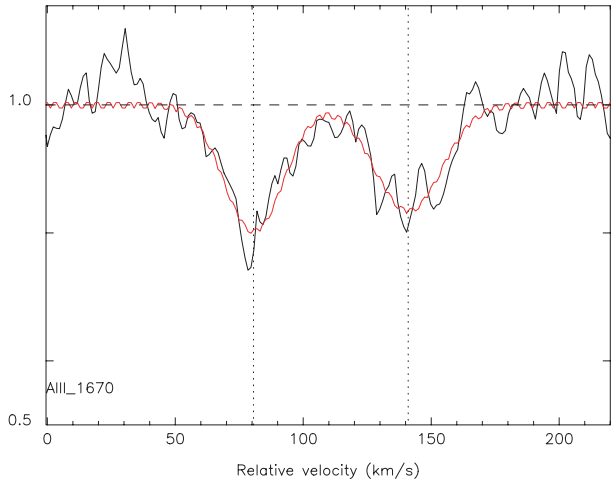

Figure 21. Fit to the low-ionization transitions of the $z_{abs} = 3.368$, log N(I) $= 19.80 \pm 0.10$ sub-DLA towards BR J2216−6714 (see Table 21).

Table 21. Parameters fitted to the low-ionization transitions of the $z_{abs} = 3.368$, log N(H I) $= 19.80 \pm 0.10$ sub-DLA towards BR J2216−6714.

z	b	log N(Al II)
3.369173	15.20 ± 2.54	11.88 ± 0.26
3.370053	17.40 ± 3.04	11.85 ± 0.27

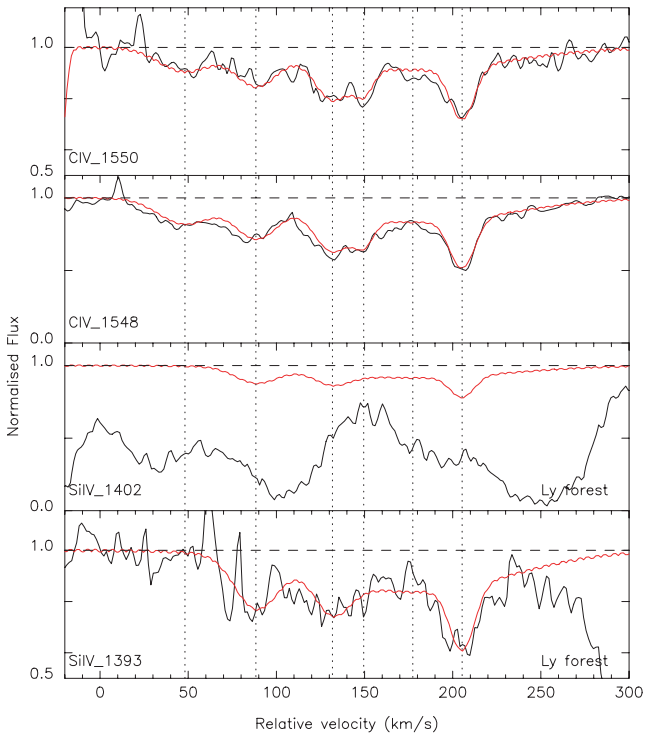

Figure 22. Fit to the high-ionization transitions of the $z_{abs} = 3.368$, log N(H I) $= 19.80 \pm 0.10$ sub-DLA towards BR J2216−6714 (see Table 22).

Table 22. Parameters fitted to the high-ionization transitions of the $z_{abs} = 3.368$, log N(H I) $= 19.80 \pm 0.10$ sub-DLA towards BR J2216−6714.

z	b	log N(C IV)	log N(Si IV)
3.368701	20.10 ± 4.07	12.95 ± 0.11	...*
3.369287	15.50 ± 2.96	13.02 ± 0.12	<12.52
3.369919	12.60 ± 5.42	13.01 ± 0.09	<12.34
3.370177	6.10 ± 1.99	12.58 ± 0.22	...*
3.370583	74.00 ± 1.59	13.49 ± 0.08	<13.09
3.370990	8.30 ± 2.01	13.03 ± 0.08	<12.48

* These components are undetected in Si IV.

sub-DLAs. The data plotted are based on the Péroux et al. (2003b) compilation with the following studies added: Dessauges-Zavadsky et al. (2004), Rao et al. (2005), Péroux et al. (2006a,b) and Meiring et al. (2007). We note that, thanks to these recent studies, the metallicity of sub-DLAs is now better constrained. These results confirm findings from Péroux et al. (2003b) that the average values of the metallicities in the various redshift bins do show more evolution with redshift for sub-DLAs than for classical DLAs. Fitting least-square regressions to the data points without including limits leads to a slope of $\alpha = -0.18$ for DLAs and of $\alpha = -0.42$ for sub-DLAs. These regression fits are plotted as dashed and solid lines (respectively) in Fig. 26. Moreover, based on Zn measurements, sub-DLAs appear more metal-rich at lower redshifts, especially at $z < 2$ (Péroux et al. 2006a,b; Meiring et al. 2007). Although our data add no new Zn measurements because of their high redshifts, it has previously been shown (Péroux et al. 2003b) that the strong evolution observed in [Fe/H] for sub-DLAs is not the result of differential depletion, given that such strong evolution is also observed in the [Zn/H] metallicity of sub-DLAs.

Instead, the difference in evolution might be explained by the fact that sub-DLAs are less prone to the biasing effect of dust and thus represent a better tool with which to detect the most metal-rich galaxies seen in absorption. Indeed, it has been suggested that the dust contained in the absorbers might introduce biases into current surveys, in the sense that the dustier systems would dim the light from the background quasar and therefore the quasar would not be taken into account in current magnitude-limited samples. In order to overcome such limitations, searches for DLAs towards radio-selected quasars have been undertaken, and the results suggest that dust obscuration might be modest (Ellison et al. 2001; Jorgenson et al. 2006). However, the samples are still small to derive firm conclusions, and some of the radio-selected quasars are actually 'dark' at optical wavelengths and could thus potentially be obscured quasars. In fact, if dust extinction in quasar absorbers is a strong function of N(Zn II) column density, as found in interstellar clouds (Vladilo 2004), the obscuration will start acting at a lower [Zn/H] ratio for DLAs than for sub-DLAs (Vladilo & Péroux 2005). In other words, we might be missing more systems in the DLA range than in the sub-DLA range, and the metal-rich sub-DLAs recently found might be the tip of the iceberg of a population that has so far gone unnoticed. A way to find metal-rich absorbers that minimizes dust effects is therefore to search for quasar absorbers with

Table 23. Total column densities for each absorber.

Quasar	z_{abs}	log N(Fe II)	log N(Si II)	log N(C II)	log N(O I)	log N(Al II)	log N(Al III)	log N(C IV)	log N(Si IV)
PSS J0118+0320[a]	4.128	14.16 ± 0.11	14.84 ± 0.13	>17.30	>16.40	...	...	14.30 ± 0.12	13.78 ± 0.12
PSS J0121+0347	2.976	13.18 ± 0.30	<13.15	<13.72	<13.98	11.93 ± 0.32	<11.77[b]	<13.79	13.33 ± 0.10
SDSS J0124+0044[a]	2.988	<13.55[c]	14.12 ± 0.12	<15.72	...	12.76 ± 0.13	...	14.43 ± 0.30	<14.20
...	3.078	<14.13	15.13 ± 0.39	>15.35	>15.15	...	...	...	...
PSS J0133+0400	3.139	...	<13.14	<13.85	...	...	<11.44[b]	...	...
...	3.995	<13.56[b,d]	13.91 ± 0.13	...	...	<11.36[b]	< 11.69[b]	<13.51	13.48 ± 0.28
...	3.999	<13.56[b]	<14.12[b]	...	...	<11.10[b]	< 11.63[b]	<13.76	<13.25
...	4.021	<13.56[b]	<14.05[b]	...	...	<11.20[b]	...	< 12.31[b]	<12.89
BRI J0137−4224	3.101	13.67 ± 0.11	14.11 ± 0.25	...	...	12.83 ± 0.42	...	13.52 ± 0.17	...
...	3.665	<13.59[b]	12.40 ± 0.13	13.14 ± 0.13	13.38 ± 0.13	<11.06[b]	< 11.96[b]	< 12.11[b]	13.06 ± 0.13
BR J2215 − 1611[a]	3.656	< 13.51[b]	<14.41[b]	...	...	...	...	<13.22	< 11.69[b]
...	3.662	<13.60[b]	13.89 ± 0.06	>14.98	15.05 ± 0.02	12.46 ± 0.45	...	13.71 ± 0.21	13.51 ± 0.05
BR J2216−6714	3.368	<13.26[b]	<13.88[b]	...	...	12.17 ± 0.26	< 11.51[b]	13.88 ± 0.10	<13.32

[a] PSS J0118+0320, $z_{abs} = 4.128$ has log N(S II) = 14.26 ± 0.11; SDSS J0124+0044, $z_{abs} = 2.988$ has log N(S II) < 14.27; BR J2215−1611, $z_{abs} = 3.656$ has log N(S II)<13.68 from a non-detection;
[b] 4σ upper limits corresponding to non-detections;
[c] log N(Fe III)<14.09 in this system;
[d] log N(Ni II)<12.31 in this system from a non-detection.

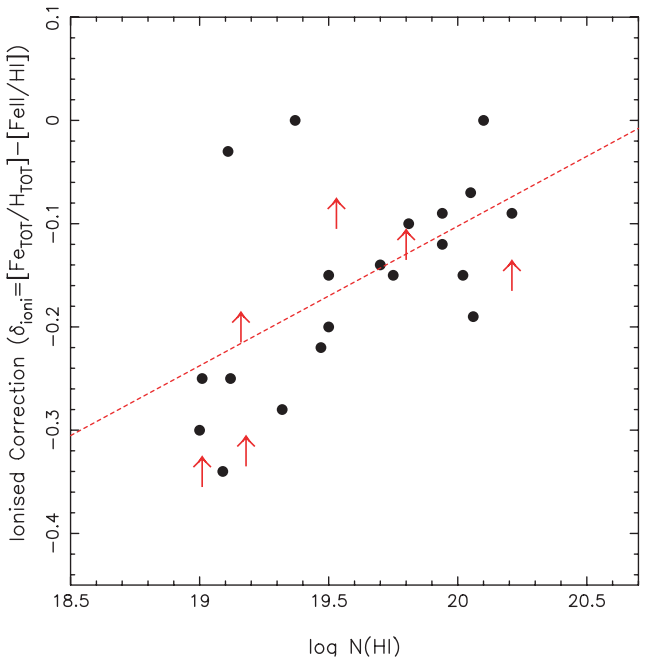

Figure 23. Ionization correction, δ_{ioni}, as a function of log N(H I) from the present study and from the literature (Prochaska et al. 1999; Dessauges-Zavadsky et al. 2003; Péroux et al. 2006a; Prochaska et al. 2006). There seems to be trend of smaller ionization corrections towards higher N_{HI}, as expected. The solid line is the linear least-squares regression with slope $\alpha = 0.13$. Upper arrows denote lower limits. Note that, in most cases, the correction, δ_{ioni}, is smaller than 0.2 dex.

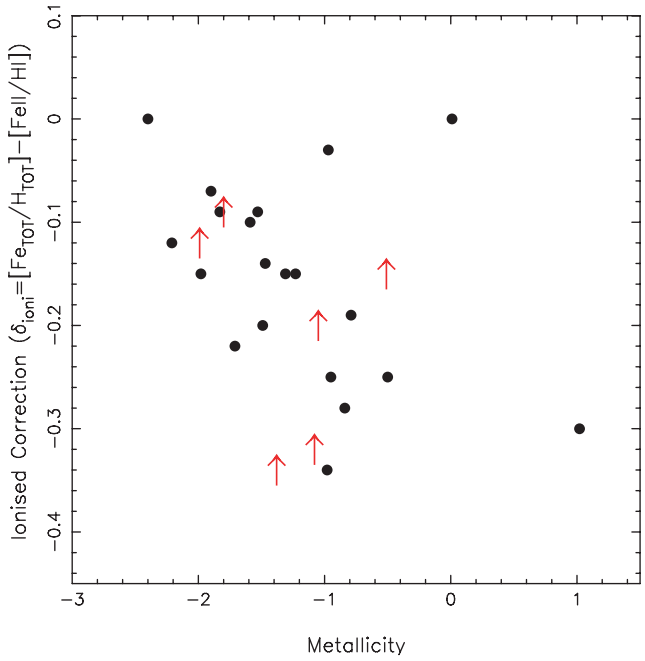

Figure 24. Ionization correction, δ_{ioni}, as a function of observed metallicity [Fe/H] (or [Si/H] when Fe measurements are not available). There is a hint of decreasing δ_{ioni} with metallicity.

relatively low N(H I) column density, such as the sub-DLAs. Another possible explanation for the metallicity difference between DLAs and sub-DLAs has recently been suggested by Khare et al. (2007). Based on the observed mass–metallicity relationship for galaxies (e.g. Tremonti et al. 2004; Savaglio et al. 2005), these authors argue that sub-DLAs may arise in massive galaxies, and DLAs in less massive galaxies.

In Fig. 27, the metallicity of both DLAs and sub-DLAs is shown as a function of log N(H I). The spread in metallicity is larger in the sub-DLA range, showing once more a strong evolution with redshift, whereas classical DLAs appear more homogeneous.

4 DISCUSSION

4.1 The missing-metals problem

A direct consequence of star-formation history is the production of heavy elements, known as metals. At high redshifts, however, our knowledge of the cosmic metal budget is still very incomplete. In fact, the amount of metals observed in high-redshift galaxies (e.g. Lyman-break galaxies, DLAs) and in the intergalactic medium was believed to be a factor of about 5 below the expected amount

Table 24. Abundances with respect to solar, [X/H], using the standard definition: $[X/H] = \log [N(X)/N(H)]_{\rm DLA} - \log [N(X)/N(H)]_{\odot}$. The error bars on [X/H] include the errors in both log $N(X)$ and log N(H I). $\delta_{\rm ioni}$ is the correction to the observed metallicity required to take into account the ionized part of the gas (see equation 1).

Quasar	$z_{\rm abs}$	log N(H I)	Fe	$\delta_{\rm ioni}$	Si	C	O	S	Al
A(X/N)$_{\odot}$	–	–	−4.55	–	−4.49	−4.10	−3.47	−4.85	−5.60
PSS J0118+0320	4.128	20.02 ± 0.15	−1.31 ± 0.26	−0.15	−0.69 ± 0.28	>1.38	>−0.15	−0.91 ± 0.26	...
PSS J0121+0347	2.976	19.53 ± 0.10	−1.80 ± 0.40	<|−0.09|	< −1.89	< −1.71	< −2.08	...	−2.00 ± 0.42
SDSS J0124+0044	2.988	19.18 ± 0.10	< −1.08	<|−0.32|	−0.57 ± 0.22	<0.64	...	< −0.06	−0.82 ± 0.23
...	3.078	20.21 ± 0.10	< −1.53	−0.09	−0.59 ± 0.49	>−0.76	>−1.59	...	...
PSS J0133+0400	3.139	19.01 ± 0.10	...	<|−0.34|	< −1.38	< −1.06	...	...	...
...	3.995	19.94 ± 0.15	< −1.83	−0.09	−1.54 ± 0.28	...	...	...	< −2.98
...	3.999	19.16 ± 0.15	< −1.05	<|−0.20|	< −0.55	...	...	...	< −2.46
...	4.021	19.09 ± 0.15	< −0.98	−0.34	< −0.55	...	...	...	< −2.29
BRI J0137−4224	3.101	19.81 ± 0.10	−1.59 ± 0.21	−0.10	−1.21 ± 0.35	...	...	...	−1.38 ± 0.52
...	3.665	19.11 ± 0.10	< −0.97	−0.03	−2.22 ± 0.23	−1.87 ± 0.23	−2.26 ± 0.23	...	< −2.45
BR J2215−1611	3.656	19.01 ± 0.15	< −0.95	−0.25	< −0.11	...	...	< −0.48	...
...	3.662	20.05 ± 0.15	< −1.90	−0.07	−1.67 ± 0.21	>−0.97	−1.53 ± 0.17	...	−1.99 ± 0.60
BR J2216−6714	3.368	19.80 ± 0.10	< −1.99	<|−0.12|	< −1.43	...	...	...	−2.03 ± 0.36

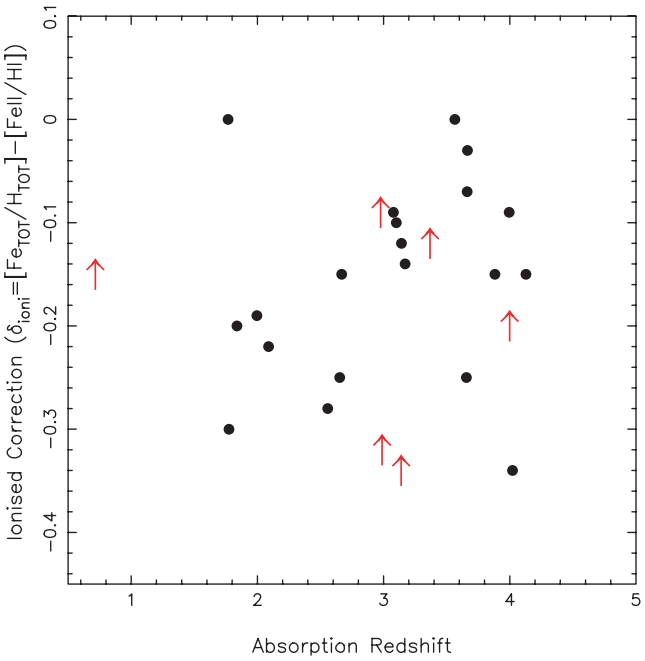

Figure 25. Ionization correction, $\delta_{\rm ioni}$, as a function of absorption redshift. Given than the incident UV background flux evolves with redshift, a correlation of the ionization corrections with $z_{\rm abs}$ is expected. No such correlation is observed.

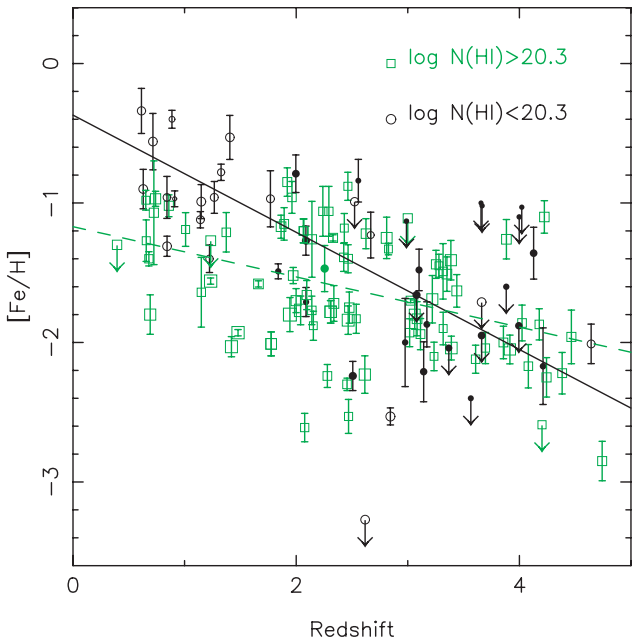

Figure 26. Redshift evolution of [Fe/H] metallicity in DLAs and sub-DLAs. Filled circles are sub-DLAs studied by our group (Dessauges-Zavadsky et al. 2003, and the present study). sub-DLAs are found to evolve more rapidly with time than DLAs, and to be more metal-rich at the lowest redshifts. The lines show the least-square regressions fitted to the data (excluding limits) for DLAs (dashed line) and sub-DLAs (solid line).

of metals produced as a result of the cosmic star-formation history. This is dubbed the 'missing-metals problem' (Pettini 1999, 2004). This census has recently been revisited in a series of papers that explores alternative populations that might contain some of the missing metals. Bouché, Lehnert & Péroux (2005) investigated the role of submillimetre galaxies, while Bouché, Lehnert & Péroux (2006) considered the Lyman-break galaxies. However, a substantial fraction of the missing metals may be hidden in very hot, collisionally ionized gas (Ferrara, Scannapieco & Bergeron 2005). Based on simple order-of-magnitude calculations, Bouché et al. (2007) discuss the possibility that the remaining missing metals could have been ejected from small galaxies by means of galactic outflows into the intergalactic medium in a hot phase that is difficult to detect using the observed properties of local galaxies. Even when taking into account the most recent observations, however, it appears that 10 to 40 per cent of metals are still missing.

Although we can measure the metallicities of DLAs up to high redshifts, the above studies found that their ad hoc metallicities are too low for them to be a major contributor to the metal budget. However, Davé & Oppenheimer (2007) used cosmological hydrodynamic simulations based on GADGET-2 to compute the redshift evolution and contribution of DLAs to the metal census. They found that their simulations reproduced the weak evolution with redshift observed in DLAs well but overproduced the metallicity at all redshifts, and suggested that highly enriched sub-DLAs might accommodate the discrepancy. In the following, we use the most recent

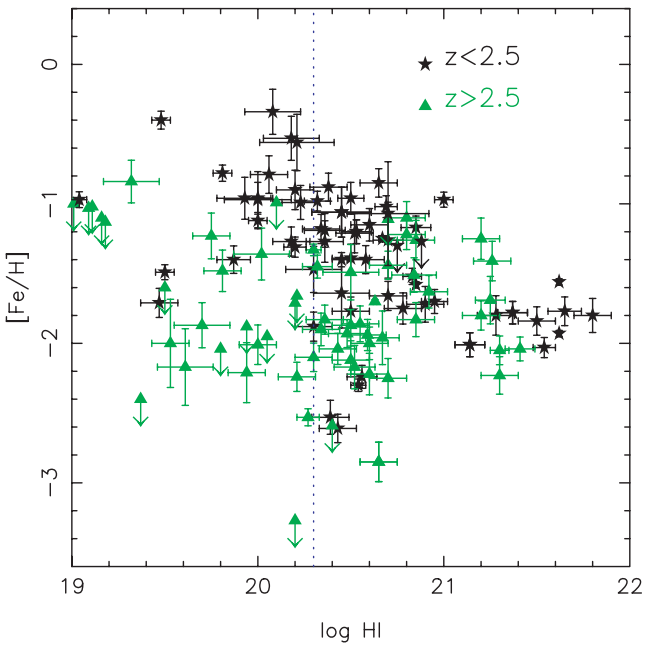

Figure 27. [Fe/H] metallicity of both DLAs and sub-DLAs as a function of log N(H I). The dotted vertical line corresponds to the DLA definition: log N(H I) > 20.3. Different redshift ranges are symbol+colour-coded and show once more the faster redshift evolution of sub-DLAs compared with DLAs.

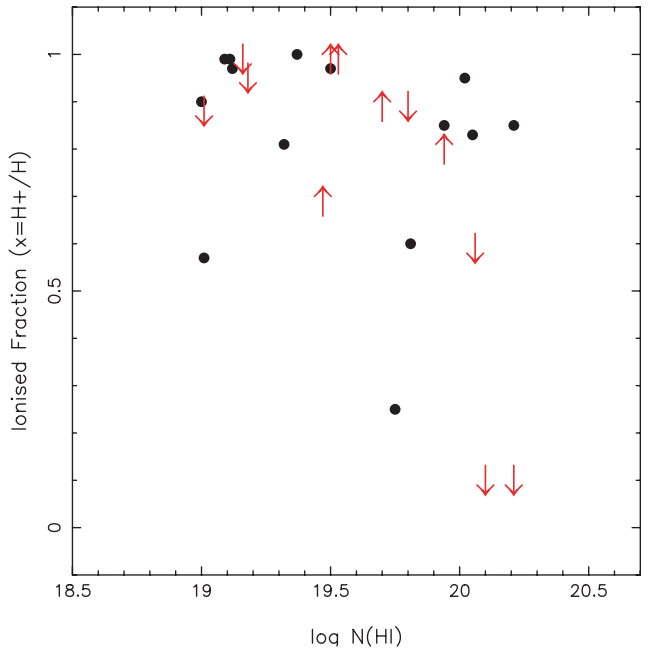

Figure 28. Ionized fraction, x=H$^+$/H$_{TOT}$, of a sample of 26 sub-DLAs as a function of N(H I) column densities. The up and down arrows denote lower and upper limits, respectively. Note that a number of x-values are found at any given N(H I) column density (see, for example, N(H I) $\sim$ 19.7).

observational data on sub-DLAs to calculate their contribution to the metal budget.

4.2 Contribution of sub-DLAs to the global metallicity

Recently, there have been several attempts to estimate the amount of metals contained in sub-DLAs (Prochaska et al. 2006), including

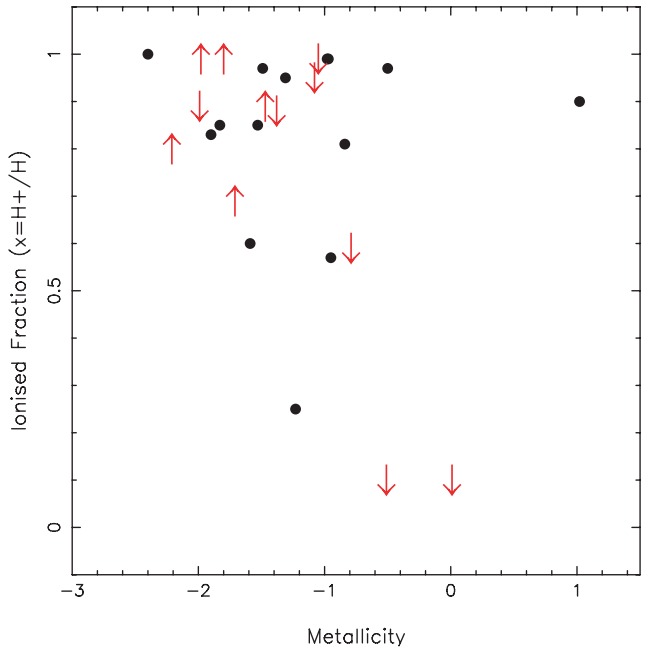

Figure 29. Evolution of the ionized fraction, x, with the metallicity, [Fe/H] (or [Si/H] when Fe measurements are not available). No obvious trend is observed.

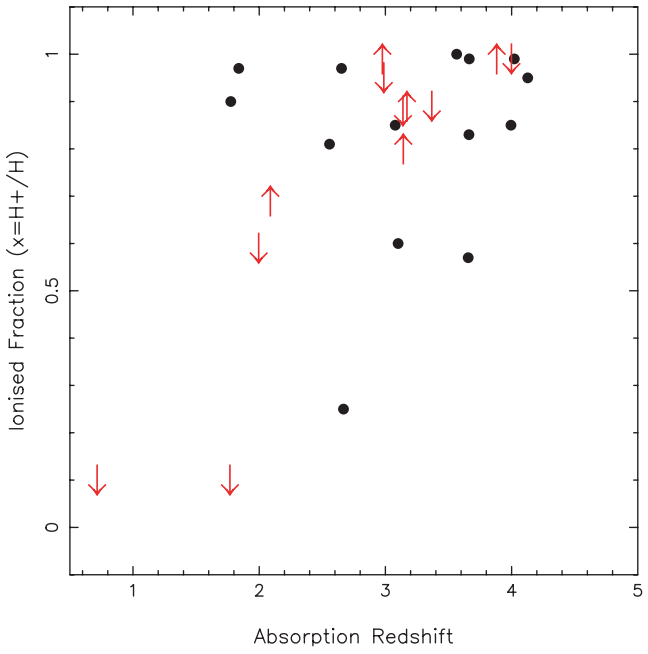

Figure 30. Evolution with cosmic time of the ionized fraction, x, in sub-DLAs.

some results based on dust-free Zn metallicity measures (Kulkarni et al. 2007). Pettini (2006) suggested that some of the missing metals might be in sub-DLAs if these were to have a significant ionized fraction. The amount of metals in the ionized gas of sub-DLAs cannot, however, be directly probed by observations. In fact, it is interesting to note that Lebouteiller et al. (2006) recently showed that the ionized gas probed in emission was more metal-rich that the neutral gas probed in absorption for most elements in a local H II

region. While the reasons for this are not yet clear, they also note that Fe II is a better tracer of neutral gas than Si III.

For high-redshift quasar absorbers, the only means to quantify the ionized fraction is to use photoionization models. The ionized fraction is defined as

$$x = \mathrm{H}^{+}/\mathrm{H}_{\mathrm{TOT}}.$$

Prochaska et al. (2006) estimated $x = 0.90$ for one sub-DLA and computed Ω_Z(sub-DLAs) using this value. Here, we use the models presented in Section 3.1 to reproduce the ionization state of 26 sub-DLAs. The x-values for these are shown in Fig. 28 as a function of N(H I) column density. A range of x-values are found at any given N(H I) column density. Fig. 29 shows the evolution of the ionization fraction with metallicity for the 26 sub-DLAs studied. No obvious trend is observed.

At $z \sim 2.5$, the amount of H I gas in sub-DLAs is measured to be $\Omega(\mathrm{H\,I}) = 0.18 \times 10^{-3}$ (Péroux et al. 2005). At the same redshifts, the metallicity of these systems measured from the undepleted Zn element is $Z/Z_{\odot} = -0.70$ (Kulkarni et al. 2007). The mean of the x-values (as opposed to the limits) at $z \sim 2.5$ is $\langle x \langle = 0.68$. Therefore, assuming that all the gas is photoionized, the observed comoving mass density of metals in sub-DLAs is

$$\Omega_Z(\text{sub-DLAs}) = \left(\frac{\langle x \rangle}{1-\langle x \rangle} + 1\right) \times 10^{-0.70} \times 0.18 \times 10^{-3} \frac{\mathrm{Z}_{\odot}}{\Omega(\mathrm{Z}_{\odot})}, \quad (3)$$

$$\Omega_Z(\mathrm{sub-DLAs}) = 2.57 \times 10^{-3}, \quad (4)$$

where $\mathrm{Z}_{\odot} = 0.0126$ by mass, and $\Omega(\mathrm{Z}_{\odot}) = \Omega_{\mathrm{baryons}} \times \mathrm{Z}_{\odot} = 5.5 \times 10^{-4}$.

The total amount of metals expected at this redshift is $\Omega(Z) = 4.5 \times 10^{-2}$. Therefore, the sub-DLAs contribute at most ∼6 per cent of the total metal in the Universe at $z \sim 2.5$ for a photoionized gas. According to recent results, if the gas were collisionally ionized, the contribution to the total amount of metals would be similar (Fox et al. 2007). So, even if sub-DLAs are mostly ionized gas, they do not close the metal budget. In fact, given that 10 to 40 per cent of the metals are still missing, the mean metallicity of sub-DLAs after ionization correction would have to be $-0.46 < Z/Z_{\odot} < +0.14$ for these systems to solve the missing-metals problem. Such metal-rich galaxies would be easily observed in emission. This is not the case for quasar absorbers, which probably probe fainter objects. Note that the higher the ionized fraction of sub-DLAs, x, the higher their contribution to the cosmic metallicity. It will thus be very important in the future to measure the ionized fraction of more sub-DLAs in order better to constrain $\langle x \rangle$ at $z \sim 2.5$.

4.3 Redshift evolution of the ionized fraction

Fig. 30 shows the evolution with cosmic time of the ionized fraction in sub-DLAs. Clearly, one would expect the ionized fraction of sub-DLAs to increase with cosmic time as the Universe becomes ionized and the meta-galactic flux increases up to $z = 1.5$. However, no clear trend seems to appear with redshift. This result supports the idea that sub-DLAs are a phase of galaxy evolution observed at various redshifts rather than a tracer of the continuous formation of galaxies and/or that we are probing different overdensities at different redshifts. In fact, systems that are more affected by higher ultra-violet flux probably have a lower observed N(H I) and are therefore not classified as sub-DLAs. Indeed, the gas cooling time is expected to be $\sim 10^9$ yr, i.e. much longer than the time it takes for H I to turn into stars ($\sim 10^7$ yr) or to be heated by the meta-galactic flux. This is also in line with the fact that only small amounts of molecular hydrogen H_2 are found in quasar absorbers (Srianand et al. 2005; Zwaan & Prochaska 2006).

5 SUMMARY

We have presented abundance and ionization-fraction determinations for a sample of 13 $z \geqslant 3$ sub-DLAs. In summary:

(i) our new high-resolution observations more than double the metallicity information for sub-DLAs previously available at $z > 3$;

(ii) results from photoionization modellings of a *sample* of 26 sub-DLAs are brought together for the first time;

(iii) the ionization correction to the observed metallicity, δ_{ioni}, is a function of the observed N(H I) column density and is smaller than 0.2 dex in most cases;

(iv) the metallicity of sub-DLAs evolves more rapidly with cosmic time and is higher than that of classical DLAs, especially at $z < 2$. This could be because sub-DLAs are less affected by the biasing effect of dust.

(v) the ionization fraction of a *sample* of 26 sub-DLAs allowed us to calculate reliably the total contribution of these systems to the so-called 'missing-metals' problem. sub-DLAs contribute no more than 6 per cent of the total amount of expected metals at $z \sim 2.5$.

ACKNOWLEDGMENTS

This paper is based on observations collected during programmes ESO 71.A-0114, ESO 73.A-0653, ESO 73.A-0071 and ESO 74.A-0306 at the European Southern Observatory with UVES on the 8.2-m KUEYEN telescope operated at the Paranal Observatory, Chile. We would like to thank Valentina D'Odorico for providing the raw spectrum of PSS J0133+0400 860 setting in advance of publication.

REFERENCES

Asplund M., Grevesse N., Sauval A. J., 2005, in Barnes T.G., III, Bash F.N., eds, ASP Conf. Ser. Vol. 336, Cosmic Abundance as Records of Stellar Evolution and Nucleosynthesis. Astron. Soc. Pac., San Francisco, p. 25
Bouché N., Lehnert M. D., Péroux C., 2005, MNRAS, 364, 319
Bouché N., Lehnert M. D., Péroux C., 2006, MNRAS, 367, L16
Bouché N., Lehnert M. D., Aguirre A., Péroux C., Bergeron J., 2007, MNRAS, 378, 525
Davé R., Oppenheimer B. D., 2007, MNRAS, 374, 427
Dessauges-Zavadsky M., Péroux C., Kim T. S., D'Odorico S., McMahon R. G., 2003, MNRAS, 345, 447
Dessauges-Zavadsky M., Calura F., Prochaska J. X., D'Odorico S., Matteucci F., 2004, A&A, 416, 79
D'Odorico V., Petitjean P., 2001, A&A, 370, 729
Ellison S. L., Yan L., Hook I. M., Pettini M., Wall J. V., Shaver P., 2001, A&A, 379, 393
Erni P., Richter P., Ledoux C., Petitjean P., 2006, A&A, 451, 19
Ferland G. J., 1997, Hazy, A Brief Introduction to CLOUDY. Univ. Kentucky Internal Report
Ferrara A., Scannapieco E., Bergeron J., 2005, ApJ, 634, L37
Fontana A., Ballester P., 1995, Messenger, 80, 37
Fox A. J., Petitjean P., Ledoux C., Srianand R., 2007, A&A, 465, 171
Jenkins E. B., Bowen D. V., Tripp T. M., Sembach K. R., 2005, ApJ, 623, 767
Jorgenson R. A., Wolfe A. M., Prochaska J. X., Lu L., Howk J. C., Cooke J., Gawiser E., Gelino D. M., 2006, ApJ, 646, 730
Khare P., Kulkarni V. P., Péroux C., York D. G., Lauroesch J. T., Meiring J. D., 2007, A&A, 464, 487

Kulkarni V. P., Khare P., Péroux C., York D. G., Lauroesch J. T., Meiring J. D., 2007, ApJ, 661, 88
Lebouteiller V., Kunth D., Lequeux J., Aloisi A., Desert J.-M., Hebrard G., Lecavelier des Etangs A., Vidal-Madjar A., 2006, A&A, 459, 161
Meiring J. D., Lauroesch J. T., Kulkarni V. P., Péroux C., Khare P., York D. G., Crotts A. P. S., 2007, MNRAS, 376, 557
Péroux C., McMahon R., Storrie-Lombardi L., Irwin M., 2003a, MNRAS, 346, 1103
Péroux C., Dessauges-Zavadsky M., D'Odorico S., Kim T. S., McMahon R., 2003b, MNRAS, 345, 480
Péroux C., Dessauges-Zavadsky M., D'Odorico S., Kim T. S., McMahon R. G., 2005, MNRAS, 363, 479
Péroux C., Kulkarni V. P., Meiring J., Ferlet R., Khare P., Lauroesch J. T., Vladilo G., York D. G., 2006a, A&A, 450, 53
Péroux C., Meiring J., Kulkarni V. P., Ferlet R., Khare P., Lauroesch J. T., Vladilo G., York D. G., 2006b, MNRAS, 372, 369
Pettini M., 1999, in Walsh J. R., Rosa M. R., eds, Proc. ESO Workshop, Chemical Evolution from Zero to High Redshift. Springer, Berlin, p. 233
Pettini M., 2004, in Esteban C., Garcĩa López R. J., Herrero A., Sànchez F., eds, XIII Canary Islands Winter School of Astrophysics, Cosmochemistry: The Melting Pot of Elements. Cambridge Univ. Press, Cambridge, p. 257
Pettini M., 2006, in Le Brun V., Mazure A., Arnouts S., Burgarella D., eds, Proc. V Marseille Internat. Cosmology Conf., The Fabulous Destiny of Galaxies: Bridging Past and Present. Frontier Group, Paris, p. 319
Pettini M., Ellison S. L., Steidel C. C., Shapley A. E., Bowen D. V., 2000, ApJ, 532, 65
Prochaska J. X., 1999, ApJ, 511, L71
Prochaska J. X., O'Meara J. M., Herbert-Fort S., Burles S., Prochter G. E., Bernstein R. A., 2006, ApJ, 648L, L97
Rao S. M., Prochaska J. X., Howk J. C., Wolfe A. M., 2005, AJ, 129, 9
Savaglio S. et al., 2005, ApJ, 635, 260
Srianand R., Petitjean P., Ledoux C., Ferland G., Shaw G., 2005, MNRAS, 362, 549
Tremonti C. et al., 2004, ApJ, 613, 898
Vladilo G., 2004, A&A, 421, 479
Vladilo G., Péroux C., 2005, A&A, 444, 461
Wolfe A., Lanzetta K. M., Foltz C. B., Chaffee F. H., 1995, ApJ, 454, 698
Zwaan M., Prochaska J., 2006, ApJ, 643, 675

This paper has been typeset from a TEX/LATEX file prepared by the author.